STANFORD UNIVERSITY

CENTER FOR SYSTEMS RESEARCH

Final Report on a Study to

PREPARE A PRELIMINARY ANALYSIS AND DESIGN DEFINITION OF A DRAG-FREE SATELLITE FOR GEODYNAMICS

Principal Investigators

Professor Benjamin O. Lange
Dr. Daniel B. DeBra
Stanford University

Professor William M. Kaula
University of California at Los Angeles

Guidance and Control Laboratory

Supported at Stanford University by the
NATIONAL AERONAUTICS AND SPACE ADMINISTRATION
under Contract NSR-05-020-379

Jerome D. Rosenberg
Geodetic Satellites Program Manager
NASA HEADQUARTERS

AUGUST 1970

FINAL REPORT ON A STUDY TO

PREPARE A PRELIMINARY ANALYSIS AND DESIGN DEFINITION

OF A DRAG-FREE SATELLITE FOR GEODYNAMICS

Principal Investigators

Professor Benjamin O. Lange
Dr. Daniel B. DeBra
Stanford University

Professor William M. Kaula
University of California
at Los Angeles

Submitted to the National Aeronautics and Space Administration

by the

Department of Aeronautics
and Astronautics
Stanford University

Institute of Geophysics
and Planetary Physics
University of California
at Los Angeles

NSR 05-020-379
Jerome D. Rosenberg
Geodetic Satellites Program Manager
NASA Headquarters

AUGUST 1970

TABLE OF CONTENTS

I. INTRODUCTION

Stanford University and the University of California at Los Angeles record in this Final Report, the results of a one-year study to prepare a preliminary analysis and design definition of a drag-free satellite for geodynamics. The work was performed under NASA contract NSR 05-020-379 which was awarded in response to our proposal [Ref. 1]. The work reported is principally in three areas. The first is the study of orbit selection and tracking requirements for determination of the temporal variations in the gravity field. The second is the development of an orbit-theory describing the short-period variations in low altitude orbits designed for determination of the higher tesseral harmonics in the spatial variations of the gravity field. The third area is satellite design. Several aspects of drag-free satellite design as applied to geodesy have been studied in detail and combined in preliminary satellite configurations.

A drag-free satellite follows an internal unsupported proof mass shielded from all external surface forces by the satellite. Since only gravitational forces act on the proof mass, it follows a purely gravitational orbit. A control system in a satellite senses the relative position of the satellite with respect to the proof mass and actuates reaction jets forcing the satellite to follow the proof mass. The satellite therefore also follows a purely gravitational orbit [Ref. 2]. This concept has been developed to a high degree at Stanford University under NASA Grant NsG 582 and was independently proposed at UCLA for aeronomy studies in 1962 [Ref. 3]. There are two principal advantages of a drag-free satellite for geodesy. First, the satellite cancels surface forces which might mask the small variations in the gravitational fields; hence, it protects the long period perturbations due to weak effects from distortion and allows them to become large enough to be measured. Secondly, the altitude of the satellite can be made lower without introducing additional disturbances to the satellite ephemeris. It is possible, therefore, to enhance the effect of the higher gravitational harmonics for either direct measurement by differentiating Doppler signals or through the long period perturbations that result from resonance-type effects.

The orbit selection analysis is presented in detail and recommendations are presented for a high altitude mission designed for determination of the temporal gravity variations. Tracking requirements have been studied for both high and low missions, and recommendations for these missions are given. An orbital theory for short period perturbations on near-circular orbits is being developed and a portion of this work is presented in this report.

The preliminary design of the drag-free satellite is significantly influenced by whether the satellite should spin or not. The primary reason for spinning is to attenuate the effect of disturbing forces on the proof mass; therefore, a study of the effect of proof mass disturbances is reported here. We have concluded the analysis and experimental verification of the feasibility of a translation control system operating on a spinning vehicle. Compatibility of a drag-free satellite control system on a spinning vehicle is therefore established.

We have also developed and simulated a special control law for spinning vehicles which allows the use of integral control in a rotating reference frame. In this way, it will be possible not only to obtain the averaging of the body-fixed disturbances on the proof mass, but also attenuate the effect of the systematic offsets of the proof mass required to actuate the control system in the presence of external disturbing forces which have a fixed orientation with respect to the orbit. These two results should relax some of the requirements for uniform distribution of mass and very tight control over the location of all parts of the satellite that are required to minimize the mass attraction disturbance to the proof mass and the gradient in this force which produces disturbances in the presence of a control system offset. An interesting coupling phenomenon in gravity stabilized drag-free satellites which was discovered and discussed in our earlier geodesy study [Ref. 4] has been investigated more thoroughly and all coupling paths that influence both the natural frequencies and the damping of the natural behavior of the vehicle have been investigated. In addition to the pitch-plane effect discussed in Ref. 4, a similar coupling mechanism in roll-yaw has been discovered and is described. We have completed two preliminary drag-free satellite designs and recommended the one which yields the simplest satellite design for the first drag-free satellite geodesy mission.

Our design work on the drag-free geodesy satellite continues to benefit from our other contracts and associations. In our role in the TRANSIT Navigation Satellite program, we have established an unusually stimulating and productive working relationship with the Applied Physics Laboratory of Johns Hopkins University [Ref. 5]. We have designed, and are building, a drag-free control system for the next TRANSIT Satellite which is expected to be launched in the middle of 1971. We have continued our work on drag-free design for a Relativity Experiment [Ref. 6], and the work on our unsupported gyro project [Ref. 7].

II. ORBITS AND TRACKING TO DETERMINE TEMPORAL VARIATIONS IN THE GRAVITY FIELD

A. INTRODUCTION

The task is to determine (1) the orbits most sensitive to variations in the tidal properties and air mass shifts in the earth; (2) the best distribution of tracking stations to measure the perturbations of the orbit resulting from these variations and mass shifts.

B. ORBIT SELECTION

1. Tidal Effects

As discussed in the Final Report for the preceding contract, the earth's tidal potential for artificial satellite perturbation can be comprehensively described by Eq. 22 in that report [Ref. 8].

$$
\begin{aligned}
T = \sum_{mpqhkj} & K_{2mpq} \left(\frac{R}{a}\right)^{k+1} F_{kmj}(I)\, G_{kj(2j-k)}(e) \\
& \bullet Q_{2hkm}\left[\varkappa_{2h}\begin{Bmatrix}\cos\\ (-1)^m \sin\end{Bmatrix}_{k\ odd}^{k\ even}\right. \\
& \left. + (k_2\epsilon)_h\begin{Bmatrix}-\sin\\ (-1)^m \cos\end{Bmatrix}_{k\ odd}^{k\ even}\right] \\
& \bullet \left[V_{kmj(2j-k)}(\omega,\ \Omega) - V^{*}_{2mpq}(\omega^{*},\ M^{*},\ \Omega^{*})\right]
\end{aligned}
\tag{1.1}
$$

All components of Eq. 1 are defined in the previous final report. For the present discussion, it can be divided into three parts:

1) those parts which are fixed by the properties of the moon's and sun's orbits, and by the product-to-sum conversion of sperical harmonics: K_{2mpq}, Q_{2hkm} and v^*_{2mpq} ;

2) those parts which depend on the tidal properties of the earth, κ_{2h} and $(k_2\epsilon)$, the coefficients of the $\underline{h}$th zonal harmonic in the Love number and phase lag, which we hope to determine from the orbit; and

3) those parts which depend on the artificial satellite orbit, $(R/a)^{k+1}F_{kmj}\ G_{kj(2j-k)}$ and $v_{km(2j-k)}$, which this study is intended to select.

To simplify Eq. 1.1, let us confine our attention to the half-dozen or so terms for the moon and sun respectively which have the largest amplitudes K_{2mpq}. Examining Table A.2 in the previous report, these terms are those for mpq of 200, 100, 110, 201, and 210. The largest omitted term, mpq 101, is less than 5% of the leading term, mpq 200.

Combining the two factors $K_{2mpq}Q_{2hkm}$, we get Table I-1.

In Table I-1, terms with $k = 1$ have been omitted because they imply a meaningless shift of the earth's center of mass, and Moon terms with $2 - 2p + q \neq 0$ have been marked with asterisks because they entail frequencies of more than one cycle/month, and hence, upon integration are not so much amplified by a small divisor. Recalling that

$$G_{\ell 0-\ell}(e) = G_{\ell\ell\ell}(e) = 0; \qquad (1.2)$$

defining the operator

TABLE I-1

FIXED FACTORS $K_{2mpq}Q_{2hkm}$ OF TIDAL DISTURBING FUNCTION

10^7 x planetary units

			hk = 02		hk = 22		hk = 42		hk = 13		hk = 33	
m	p	q	Moon	Sun	Moon	Sun	Moon	Sun	Moon	Sun	Moon	Sun
1	0	0	.441*	.213	.210*	.102	-.084*	-.041	.176*	.085	---	---
1	1	0	-.427	-.206	-.204	-.099	.081	.040	-.170	-.082	---	---
2	0	0	2.12*	1.03	-.606*	-.295	.101*	.049	.424*	.206	-.283*	-.138
2	0	1	.409*	.061	-.117*	-.017	.019*	.003	.082*	.012	-.055*	-.008
2	1	0	.186	.089	-.053	-.025	.009	.004	.037	.018	-.025	-.012

$$K_{hkm} = \varkappa_{2h}\begin{Bmatrix}\cos\\(-1)^m\sin\end{Bmatrix}_{k\ odd}^{k\ even} + (k_2\epsilon)_h\begin{Bmatrix}-\sin\\(-1)^m\cos\end{Bmatrix}_{k\ odd}^{k\ even}; \tag{1.3}$$

and writing out $v_{kmj(2j-k)}$ and v^*_{2mpq}, we get as our working potential:

terms h = 0:

$$\begin{aligned}10^7 \times T_0 = {} & 2.12F_{221}G_{210}\left(\frac{R}{a}\right)^3 M_{022}\left\{-2\left(\omega_{\mathfrak{D}}+M_{\mathfrak{D}}\right) + 2\left(\Omega-\Omega_{\mathfrak{D}}\right)\right\}\\ & + 1.03F_{221}G_{210}\left(\frac{R}{a}\right)^3 M_{022}\left\{-2\left(\omega_{\odot}+M_{\odot}\right)+ 2\Omega\right\}\\ & -0.427F_{211}G_{210}\left(\frac{R}{a}\right)^3 M_{021}\left\{\Omega-\Omega_{\mathfrak{D}}\right\}\\ & +0.213F_{211}G_{210}\left(\frac{R}{a}\right)^3 M_{021}\left\{-2\left(\omega_{\odot}+M_{\odot}\right) + \Omega\right\}\\ & -0.206F_{211}G_{210}\left(\frac{R}{a}\right)^3 M_{021}\Omega;\end{aligned} \tag{1.4}$$

terms h = 1:

$$\begin{aligned}10^7 \times T_1 = {} & 0.206\Big[F_{321}G_{31-1}\left(\frac{R}{a}\right)^4 M_{132}\left\{\omega-2\left(\omega_{\odot}+M_{\odot}\right) + 2\Omega\right\}\\ & + F_{322}G_{321}\left(\frac{R}{a}\right)^4 M_{132}\left\{-\omega-2\left(\omega_{\odot}+M_{\odot}\right) + 2\Omega\right\}\Big]\\ & - 0.170\Big[F_{311}G_{31-1}\left(\frac{R}{a}\right)^4 M_{131}\left\{\omega+\Omega-\Omega_{\mathfrak{D}}\right\}\\ & + F_{312}G_{321}\left(\frac{R}{a}\right)^4 M_{131}\left\{-\omega+\Omega-\Omega_{\mathfrak{D}}\right\}\Big];\end{aligned} \tag{1.5}$$

terms h = 2:

$$10^7 \times T_2 = -0.606F_{221}G_{210}\left(\frac{R}{a}\right)^3 M_{222}\left\{-2\left(\omega_\oplus+M_\oplus\right) + 2\left(\Omega-\Omega_\oplus\right)\right\}$$

$$- 0.295F_{221}G_{210}\left(\frac{R}{a}\right)^3 M_{222}\left\{-2\left(\omega_\odot+M_\odot\right) + 2\Omega\right\}$$

$$- 0.204F_{211}G_{210}\left(\frac{R}{a}\right)^3 M_{221}\left\{\Omega-\Omega_\oplus\right\} \qquad (1.6)$$

$$+ 0.102F_{211}G_{210}\left(\frac{R}{a}\right)^3 M_{221}\left\{-2\left(\omega_\odot+M_\odot\right) + \Omega\right\}$$

$$- 0.099F_{211}G_{210}\left(\frac{R}{a}\right)^3 M_{221}\Omega;$$

terms h = 3:

$$10^7 \times T_3 = -0.138\Big[F_{321}G_{31-1}\left(\frac{R}{a}\right)^4 M_{332}\left\{\omega-2\left(\omega_\odot+M_\odot\right) +2\Omega\right\} \qquad (1.7)$$

$$+ F_{322}G_{321}\left(\frac{R}{a}\right)^4 M_{332}\left\{-\omega-2\left(\omega_\odot+M_\odot\right) + 2\Omega\right\}\Big];$$

and terms h = 4:

$$10^7 \times T^4 = 0.081F_{211}G_{210}\left(\frac{R}{a}\right)^3 M_{421}\left(\Omega-\Omega_\oplus\right). \qquad (1.8)$$

Note in Eqs. 1.4 and 1.6 that terms with the same value of m have the same ratio of amplitudes, but that the ratio differs for m = 1 and m = 2. Hence, from a single satellite, there seems to be hope to separate T_2 from T_o and T_3 from T_1.

Since the exponents on (R/a) are small, we can allow a semi-major axis a large enough to permit a big eccentricity e to determine T_1 and T . The choice of inclination I then should make

(1) the factors F_{kmj} and dF_{kmj}/dI large; and

(2) the rates $(k-2j)\dot{\omega} + m\dot{\Omega}$ small, for terms other than the lunar mpq = 200.

Since

$$\frac{\dot{\omega}}{\dot{\Omega}} \approx \frac{1 - 5\cos^2 I}{2\cos I}, \tag{1.9}$$

inclinations for zero rates are

$\dot{\Omega}$: 90°

$\dot{\omega}+2\dot{\Omega}$: 0° or 101.5°

$-\dot{\omega}+2\dot{\Omega}$: 78.5° or 180°,

$\dot{\omega}+\dot{\Omega}$: 46° or 107°; and

$-\dot{\omega}+\dot{\Omega}$: 73° or 134°.

The inclination functions $F_{\ell mp}$, with inclinations for maximum $F_{\ell mp}$ and $\partial F_{\ell mp}/\partial I$:

$$\begin{aligned}
F_{311} &= -3 \sin I \cos I/2: && 45°,135°;0°,90° \\
F_{331} &= 3 \sin^2 I/2 && 90°;45°,135° \\
F_{311} &= 15 \sin^2 I(1+3 \cos I)/16 && 0°,70°;35°,90° \\
&\quad - 3(1+\cos I)/4: && \\
F_{312} &= 15 \sin^2 I(1-3 \cos I)/16 && 40°;0°,90° \\
&\quad - 3(1 - \cos I)/4 && \\
F_{321} &= 15 \sin I(1-2 \cos I-3 \cos^2 I)/8: && 35°;0°,72° \\
F_{322} &= -15 \sin I(1+2 \cos I-3 \cos^2 I)/8: && 72°;45°,90°
\end{aligned} \tag{1.10}$$

An inclination around 70° - 75° thus seems preferable for a first satellite, and around 45° for a second satellite. Since

$$G_{s1-1} = G_{s21} = e(1-e^2)^{-5/2}, \tag{1.11}$$

an inclination at least 0.25 seems desirable to determine the odd zonal harmonics in the tidal properties. Then, assuming a perigee height of at least 800 km for good tracking coverage,

$$a/R > 1.5 \tag{1.12}$$

This produces a significant damping factor $(R/a)^4$ of less than 0.2. It therefore should be examined whether the absolute magnitude of these tidal perturbations are larger than the anticipated errors in the gravity field which might alias the tidal effects.

The perturbations which will be used the most, even if the satellite is drag free, are those of the orientation of the orbital plane, $\Delta\Omega$ and ΔI. For ΔI, the usual Lagrangian planetary equation

$$\dot{I} = \frac{1}{na^2(1-e^2)^{\frac{1}{2}}}\left[\frac{\partial T}{\partial \omega}\cot I - \frac{\partial T}{\partial \Omega}\csc I\right], \tag{1.13}$$

where n is the mean motion, $\mu^{\frac{1}{2}}a^{-3/2}$.

Substituting Eqs. 1.1 and 1.3 for T and integrating

$$\Delta I = \frac{1}{na^2(1-e^2)^{\frac{1}{2}}} \sum_{mpqhkj} K_{2mpq}\left(\frac{R}{a}\right)^{k+1} F_{kmj} G_{kj(2j-k)} Q_{2hkm} \tag{1.14}$$

$$\bullet \frac{(k-2j)\cot I - m \csc I}{\dot{v}_{kmj(2j-k)} - \dot{v}^*_{2mpq}} M_{hkm}\left(v_{kmj(2j-k)} - v^*_{2mpq}\right)$$

The largest term for all but polar satellites probably would be the second in T_o, Eq. 1.4, mpqhkj = 200021. Substituting from Eq. 1.4, and writing out $F_{221}G_{210}$

$$\Delta I_{200021} = \frac{-1.54 \times 10^{-7}}{na^2(1-e^2)^2}\left(\frac{R}{a}\right)^3 \frac{\sin I}{\dot{\Omega}-\dot{\omega}_\odot-\dot{M}_\odot} \bullet M_{022}\left\{2\left(\Omega-\omega_\odot-M_\odot\right)\right\} \tag{1.15}$$

The nodal motion

$$\dot{\Omega} = \frac{3n\ J_2}{2(1-e^2)^2}\left(\frac{R}{a}\right)^2 \cos I \tag{1.16}$$

For a/R = 1.5, e = 0.25, $I = 72.5°$, $\dot{\Omega}$ will be -0.0000895 in "planetary" units, radians/806.8 sec: or -0.55°/day; J_2 is 0.001083; $\dot{\omega}_\odot + M_\odot$ is about 0.99°/day, or 0.0001607. Hence

$$\Delta I_{200021} = 1.62 \times 10^{-4} M_{022}\left\{2\left(\Omega-\omega_\odot-M_\odot\right)\right\} \tag{1.17}$$

with period 360°/2 (0.55° + 0.99°) = 117 days.

The expected magnitude of M_{022} is 0.3 cos - 0.03 sin, whence the amplitude of ΔI_{200021} will be 0.49×10^{-4} rad, or 10 arc sec, or 460 meters. The phase lag effect then will be about 40 meters.

The largest effect of north-south asymmetry in tidal properties on the 72.5° orbit will depend very much on the rate. The perigee motion

$$\dot{\omega} = \frac{3n\ J_2}{4(1-e^2)^2}\left(\frac{R}{a}\right)^2 (5\cos^2 I - 1) = -.0000814, \tag{1.18}$$

whence

$$\dot{\omega} - 2\left(\dot{\omega}_{\odot}+\dot{M}_{\odot}\right) + 2\dot{\Omega} = -.0005818 = -3.56^{\circ}/\text{day}$$

$$-\dot{\omega} - 2\left(\dot{\omega}_{\odot}+\dot{M}_{\odot}\right) + 2\dot{\Omega} = -.0004190 = -2.56^{\circ}/\text{day} \qquad (1.19)$$

$$\dot{\omega} + \dot{\Omega} - \dot{\Omega}_{\mathfrak{D}} = -.0001723 = -1.05^{\circ}/\text{day}$$

$$-\dot{\omega} + \dot{\Omega} - \dot{\Omega}_{\mathfrak{D}} = .0000005 = .00/\text{day}$$

The last of these effects will be too close to secular to make it readily distinguishable. Referring to Eq. 1.10, we see F_{311} is close to a maximum, so that the third effect, of 342 day period, seems most interesting. Substituting from Eqs. 1.5, 1.10, 1.11 in Eq. 1.14

$$\Delta I_{110131} = -0.17 \times 10^{-7} \frac{e}{na^2(1-e^2)^3}\left(\frac{R}{a}\right)^4$$

$$\bullet \left[\frac{15}{16}\sin^2 I(1+3\cos I) - \frac{3}{4}(1+\cos I)\right] \qquad (1.20)$$

$$\bullet \frac{\cot I - \csc I}{\dot{\omega} + \dot{\Omega} - \dot{\Omega}_{\mathfrak{D}}} M_{131}\left(\omega+\Omega-\Omega_{\mathfrak{D}}\right)$$

For $a/R = 1.5$, $e = 0.25$, $I = 72.5^{\circ}$,

$$\Delta I_{110131} = -2.3 \times 10^{-6} M_{131}\left(\omega+\Omega-\Omega_{\mathfrak{D}}\right) \qquad (1.21)$$

The largest magnitude of M_{131} we might reasonably expect is 0.03 sin - 0.01 cos, whence the amplitude of ΔI_{110131} will be 7.0×10^{-8} rad, or 0.015 arc sec, or 0.8 meters, and the phase lag effect about 0.3 meters. As indicated by Table I-1, these effects will be enhanced by the sun almost 50% in a term differing in rate by $\dot{\Omega}_{\mathfrak{D}}$.

The expected ΔI_{110131} is thus too small for an almost annual period to be confident about distinguishing it. There does not seem much hope by reducing the eccentricity, and hence, the semi-major axis. If we assume the perigee radius to be fixed, then the semi-major axis a will be proportionate to $(1-e)^{-1}$ and from Eqs. 1.16, 1.18, 1.20, the ΔI_{110131} dependence on eccentricity will be

$$\Delta I_{110131} \propto \frac{e}{(1-e^2)^3(1-e)^{-9/2}} \cdot \frac{1}{(1-e^2)^{-2}(1-e)^{7/2}}$$

$$= \frac{e}{1+e} \tag{1.22}$$

which is an increasing function of eccentricity.

Hence, perhaps the attempt to determine the asymmetric variation in tidal properties should be anandoned in favor of optimizing for determining the symmetric variation, whose leading effect would be through either the second or third term in Eq. 1.6, mpqhkj 200221 or 110221. Substituting in Eq. 1.14

$$\Delta I_{200221} = \frac{-0.462 \times 10^{-7}}{na^2(1-e^2)^2}\left(\frac{R}{a}\right)^3 \frac{\sin I}{\dot{\Omega} - \dot{\omega}_\odot - \dot{M}_\odot} M_{222}\left\{2\left(\Omega - \omega_\odot - M_\odot\right)\right\}; \tag{1.23}$$

$$\Delta I_{110221} = \frac{-0.306 \times 10^{-7}}{na^2(1-e^2)^2}\left(\frac{R}{a}\right)^3 \frac{\cos I}{\dot{\Omega} - \dot{\Omega}_\mathbb{D}} M_{221}\left(\Omega - \Omega_\mathbb{D}\right)$$

$$\approx 0.188 \times 10^{-4} M_{221}\left(\Omega - \Omega_\mathbb{D}\right), \tag{1.24}$$

using Eq. 1.16 and Kepler's law. For a polar orbit of zero eccentricity,

$$\Delta I_{200221} = \frac{0.288 \times 10^{-3}}{na^2}\left(\frac{R}{a}\right)^3 M_{222}\left\{2\left(\Omega - \omega_\odot - M_\odot\right)\right\}, \tag{1.25}$$

in planetary units. For an a/R of 1.15,

$$\Delta I_{200221} = 0.177 \times 10^{-3} M_{222} \left\{ 2\left(\Omega - \omega_{\odot} - M_{\odot}\right)\right\}. \tag{1.26}$$

Taking 0.03 cos - 0.01 sin as the largest magnitude of M_{222} which might be expected, the amplitude of ΔI_{200221} will be 0.5×10^{-5}, or 1.0 arc sec, or 40 meters, and the phase lag effect about 15 meters.

Given a drag-free system, it is worthwhile to explore further the in-plane perturbations. At the precision entailed for these tidal effects, the drag-free capability is still necessary to eliminate radiation pressure in orbits too high to be affected significantly by the atmosphere. The eccentricity effect

$$\dot{e} = \frac{(1-e^2)^{\frac{1}{2}}}{na^2 e} \cdot \frac{\partial T}{\partial \omega} \tag{1.27}$$

Substituting Eqs. 1.1 and 1.13 for T and integrating

$$\Delta e = - \frac{(1-e^2)^{\frac{1}{2}}}{na^2 e} \sum_{mpqhkj} K_{2mpq} \left(\frac{R}{a}\right)^{k+1} F_{kmj} G_{kj(2j-k)} \tag{1.28}$$

$$\bullet\ Q_{2hkm} \frac{k - 2j}{\dot{v}_{kmj(2j-k)} - \dot{v}^*_{2mpq}} M_{hkm} \left(v_{kmj(2j-k)} - v^*_{2mpq}\right)$$

Eq. 1.28 differs from Eq. 1.14 by a factor

$$\frac{(k-2j)(1-e^2)\sin I}{[m - (k-2j)\cos I]e}$$

Applying this factor to the asymmetric case mpqhkj = 110131, Eq. 1.20, we get

$$\Delta e_{113101} = \frac{-0.17 \times 10^{-7}}{na^3(1-e^2)^2}\left(\frac{R}{a}\right)^4\left[\frac{15}{16}\sin^2 I(1+3\cos I) - \frac{3}{4}(1+\cos I)\right]$$

$$\bullet \frac{1}{\dot{\omega} + \dot{\Omega} - \dot{\Omega}_{\odot}} M_{131}\left(\omega+\Omega-\Omega_{\odot}\right) \tag{1.29}$$

For $a/R = 1.5$, $e = 0.25$, $I = 72.5°$,

$$\Delta e_{110131} = -1.2 \times 10^{-5} M_{131}\left(\omega+\Omega-\Omega_{\odot}\right), \tag{1.30}$$

about five times as large as the inclination effect, Eq. 1.21. Furthermore, for $a/R = 1.15$, $e = 0.00$,

$$\Delta e_{110131} = -4.3 \times 10^{-5} M_{131}\left(\omega+\Omega-\Omega_{\odot}\right), \tag{1.31}$$

or about 14 meters amplitude and 5 meters phase lag effect for the maximum likely M_{131} of 0.03 sin - 0.01 cos, adding 50% for the solar effect.

In any case, it seems clear that the orbit should not have significant eccentricity, should have appreciable inclination, 70° to 90°, and be of a minimum attitude compatible with good observational coverage, say, 1000 km.

2. Air Mass Shift Effects

For purposes of satellite orbit perturbation, such mass shifts can be expressed as a surface density layer σ in terms of zonal harmonics

$$\sigma = \sum_{il}\left\{C_{il}\cos f_i t + S_{il}\sin f_i t\right\}P_{l0}(\sin\varphi) \tag{1.32}$$

where f_i is frequency in radians per unit time.

The corresponding potential A, using the standard formulae for a

surface layer effect:

$$A = 4\pi GR \sum_{i\ell} \frac{(R/r)^{\ell+1}}{2\ell+1} \left\{ C_{i\ell} \cos f_i t + S_{i\ell} \sin f_i t \right\} P_{\ell,0}(\sin\vartheta) \quad (1.33)$$

Applying the usual transformation to Kepler elements, the resulting long-periodic terms

$$A = 2\pi GR \sum_{i\ell} \frac{(R/a)^{\ell+1}}{2\ell+1} \sum_{p=1}^{\ell-1} F_{\ell op} G_{\ell m(2p-\ell)} \left[N_{1i\ell} \psi_{1i\ell p} + N_{2i\ell} \psi_{2i\ell p} \right], \quad (1.34)$$

where the angles $\psi_{ji\ell p}$ are

$$\begin{aligned} \psi_{1i\ell p} &= f_i t + (\ell-2p)\omega \\ \psi_{2i\ell p} &= f_i t - (\ell-2p)\omega; \end{aligned} \quad (1.35)$$

and the operators $N_{ji\ell p}$ are

$$N_{1i\ell} = C_{i\ell} \begin{Bmatrix} \cos \\ \sin \end{Bmatrix}_{\ell\ \text{odd}}^{\ell\ \text{even}} + S_{i\ell} \begin{Bmatrix} \sin \\ -\cos \end{Bmatrix}_{\ell\ \text{odd}}^{\ell\ \text{even}} \quad (1.36)$$

$$N_{2i\ell} = C_{i\ell} \begin{Bmatrix} \cos \\ -\sin \end{Bmatrix}_{\ell\ \text{odd}}^{\ell\ \text{even}} + S_{i1} \begin{Bmatrix} \sin \\ \cos \end{Bmatrix}_{\ell\ \text{odd}}^{\ell\ \text{even}}$$

Using Eqs. 1.13 and 1.27, we get the resulting perturbations of the inclination and eccentricity

$$\Delta I = \frac{2\pi GR}{na^2(1-e^2)^{\frac{1}{2}}} \cot I \sum_{i\ell pj} \frac{(R/a)^{\ell+1}}{2\ell+1} F_{\ell op} \quad (1.37)$$

$$\bullet\ G_{\ell p(2p-\ell)} \frac{(\ell-2p)}{\psi_{ji\ell p}} N_{ji\ell p} \psi_{ji\ell p}$$

$$\Delta e = \frac{2\pi GR}{na^2 e}(1-e^2)^{\frac{1}{2}} \sum_{i\ell pj} \frac{(R/a)^{\ell+1}}{2\ell+1} F_{\ell op}$$

(1.37) cont

$$\bullet\ G_{\ell p(2p-\ell)}\ \frac{(\ell-2p)}{\Psi_{ji\ell p}} N_{ji\ell p} \Psi_{ji\ell p}$$

Similar to even degree zonal harmonics in the earth's fixed gravity field, even degree zonal harmonics in the time-varying gravity will not have a perceptible effect on the action elements of a circular orbit. Hence, we are interested in effects on the angle elements, in particular, the node

$$\dot{\Omega} = \frac{\csc I}{na^2(1-e^2)^{\frac{1}{2}}} \cdot \frac{\partial A}{\partial I}$$

$$\Delta\Omega = \frac{2\pi GR}{na^2(1-e^2)^{\frac{1}{2}}} \csc I \sum_{i\ell pj} \frac{(R/a)^{\ell+1}}{2\ell+1} \tag{1.38}$$

$$\bullet\ \frac{\partial F_{\ell op}}{\partial I} G_{\ell p(2p-\ell)} \frac{\bar{N}_{ji\ell p} \Psi_{ji\ell p}}{\Psi_{ji\ell p}} \tag{1.39}$$

where $\bar{N}_{ji\ell p}\Psi_{ji\ell p}$ is the integral of $N_{ji\ell p}\Psi_{ji\ell p}$ with respect to $\Psi_{ji\ell p}$.

Maps of seasonal variation in air pressure [Ref. 9] suggest that the annual variation could have magnitudes on the order of a millibar for the second and third zonal harmonics. Neglecting phase, this suggests for Eq. 1.32, $\ell = 1,2$:

$$C_{1\ell} = \frac{\Delta p_\ell}{g} \approx \frac{10^{-3} \times 10^6}{10^3} = 1 = .034 \times 10^{-9} \text{ plan. u.} \tag{1.40}$$

$$f_1 = 1 \text{ cycle year} = 1.6 \times 10^{-4} \text{ plan. u.}$$

where "plan. u." refers to a system where G = 1, earth's R, M = 1.

The leading effect of the second zonal harmonic will be on the node with $\ell p = 21$

$$\Delta\Omega_{121} = \frac{2\pi GR}{5na^2(1-e^2)^{\frac{1}{2}}}\csc I\left(\frac{R}{a}\right)^3\frac{\partial F_{201}}{\partial I}G_{210}\frac{C_{12}\sin f_1 t}{f_1}$$

$$= \frac{3\pi GR}{5na^2(1-e^2)^2}\left(\frac{R}{a}\right)^3\cos I\frac{C_{12}\sin f_1 t}{f_1} \qquad (1.41)$$

$$= \frac{0.4\times 10^{-8}}{na^2(1-e^2)^2}\left(\frac{R}{a}\right)^3\cos I \sin 1.6\times 10^{-4}t$$

For a/R = 1.15, e = 0.00, I = 72.5° ,

$$\Delta\Omega_{121} = 7.4\times 10^{-8}\sin 1.6\times 10^{-4}t$$

i.e., an effect of 0.015 arc sec or 0.5 meters.

As discussed by Munk & MacDonald [Ref. 9], however, the annual variation of rotation of the earth would require a C_{12} about 15 times as large as if it were due to mass shifts, so its effect on the node would be about 8 meters.

C. TRACKING STATION DISTRIBUTION

The tidal effects analysis indicated that (1) a fairly high inclination would be desirable, and that (2) since only very low degree harmonic effects will be perceptible, the orbit can be fairly high. Consideration (1) requires that the tracking stations be well-distributed in latitude, but (2) that there need not be a great number of stations. Distribution in longitude is also desirable so that the tidal and mass shift effects will not be aliased by errors in tesseral harmonic coefficients of the gravitational field. The orbital period

should, of course, avoid commensurability with the earth's rotation. Since the errors in the latest determination of non-resonant tesserals by Gaposhkin & Lambeck are equivalent to errors of a meter or less in orbital oscillations of one cycle of more per day, these effects will probably be less serious than those of errors in the fixed zonal harmonics. The latter we should hope to discriminate by analyzing data over a long enough span that the oscillations of the tidal and mass shift effects dependent on the motion of the node ($\dot{\Omega}$) and the rates of the forcing functions ($\omega_{\odot} + M_{\odot}$, f_i, etc.) going through complete cycles.

The foregoing suggests that as few as six tracking stations might suffice, provided that they were uniformly spaced over the globe--say at latitudes of about 40° in each hemisphere, spaced at 120° intervals in longitude.

D. NUMERICAL ANALYSIS

The computer programs being developed in connection with Contract NGR 05-007-280, Error Analysis of Earth Physics Satellite Systems, have been adapted to make a more detailed analysis of orbit selection and tracking station distribution for determination of the temporal variations in the gravitational field. The essential procedure is to calculate the normal equations arising from analysis of a hypothetical series of observations, and to invert these normals to determine the standard deviations and correlation coefficients of the parameter sought. Only by such analysis can effects which are stochastic (such as weather) or awkward to express in Fourier series (such as nonuniform station distribution) be estimated.

E. CONCLUSIONS

This study indicates that the use of the drag-free capability to determine temporal variations of the gravity field is quite distinct from its use to improve knowledge of the spatial variations in the field. For the temporal variations, we wish to cancel out surface

forces over a long time on the order of a year, and the low harmonic degree of the effects allows the relatively high altitude desirable not only to enable long term drag-free performance, but also to give ground tracking coverage. For the spatial variations, we wish to push the satellite to as low an altitude as possible, in order to sense as short wavelength effects as possible. Satellite-to-satellite tracking is essential, and the orbit can be short-lived: long enough to yield a spacing of equator crossings equal to the half-wavelength we aspire to resolve: $20,000/(16 \times 250)$ = five days initially, $20,000/(16 \times 100)$ = 13 days eventually, if a circular orbit; as many weeks, if eccentric.

It is therefore recommended that to determine temporal variations in the gravity field:

(1) The orbit be

a) of inclination 70° to 80° (to get at least one revolution of the node in a year);

b) nearly circular;

c) of 1050 km altitude (period 106.4 min., avoiding commensurability with anything less than a 27^{th} degree tesseral harmonic).

(2) The drag-free capability last at least one year.

(3) The tracking be from a distant satellite, if possible. But if from the ground, the stations should be well distributed, say, at least one per 90° × 90° × 90° quadrant of the globe.

These recommendations will be refined by the numerical error analysis, which is also being applied to the question of circular vs eccentric for a minimum altitude drag-free satellite designed to determine the spatial variations. These analyses will test tracking distributions of likely realization, such as those suggested by the ISAGEX project.

Since the satellite recommended herein will have global coverage and a well-determined orbit, it is suggested that it be considered for tracking of, and data relay from, ocean buoys, <u>if</u> significant economy in buoy transmitter power or tracking accuracy (compared to a geosynchronous satellite) would result.

III. ORBIT ANALYSIS

List of Symbols

a	semi-major axis
$c_{\ell m}$	earth gravity coefficient
f	true anomaly
F	disturbing function
h	$\sqrt{\mu a}\ (1-\epsilon^2)^{\frac{1}{2}}$
i	inclination
I_M	inclination of lunar orbit with respect to the equator
I_s	inclination of solar orbit with respect to the equator
$\bar{J}_2$	$3/2\ J_2(R_o\mu/h^2)^2$
$J_{\ell m}$	earth gravity coefficient
ℓ_M	mean position of moon as measured from perigee
ℓ_s	mean position of sun as measured from point of closest approach
M	mean anomaly
r	distance to satellite
r_M	semi-major axis of moon's orbit
r_s	semi-major axis of earth's orbit about sun
R	radius of earth
R_e	portion of disturbing function due to the earth

R_M portion of disturbing function due to the moon

R_s portion of disturbing function due to the sun

$S_{\ell m}$ earth gravity coefficient

u $M + \omega$

U' $f + \omega$

β intrack fluctuation

δ latitude

ϵ eccentricity of satellite's orbit

ϵ_M eccentricity of moon's orbit

ϵ_s eccentricity of earth's orbit about sun

ξ $\epsilon \cos \omega$

η $\epsilon \sin \omega$

θ_E $\omega_o t$

θ_M $\ell_M + \omega_M$

θ_s $\ell_s + \omega_s$

μ mass parameter of earth

μ_M mass parameter of moon

μ_s mass parameter of sun

ρ $1/r$

σ cross-track fluctuation

φ longitude

$\varphi_{\ell m}$ constant

$\psi_{\ell m}$ constant

Ω position of node

Ω_M position of node of lunar orbit with respect to earth

ω perigee position

ω_M location of perigee of moon's orbit with respect to earth

ω_o earth rotation rate

ω_s location of pericenter of earth's orbit with respect to sun.

A. INTRODUCTION

As a result of the Williamstown meeting, a drag-free geodetic satellite will very likely be placed into a nearly circular orbit with an eccentricity of less than 10^{-2}. A radar altimeter may be carried on the same flight.

The nongravitational errors in the drag-free satellite system are less than 10^{-10} g; however, the uncertainty in the geopotential is of the order 10^{-7} g. Therefore, it is the purpose of this study to develop an accurate orbit theory that is valid in principle for an extended period of time (10^3 rev.), and includes all gravitational forces up to at least 10^{-8} g.

The short period position and velocity fluctuations are computed to second order in J_2 and mean eccentricity. Thus, fluctuations involving J_2, J_2^2, and ϵJ_2 as well as the zonal and tesseral harmonic coefficients $J_{\ell m}$ are retained. The lunar-solar gravitational effects for zero eccentricity are also included. Omitted from the short-period fluctuations are all terms containing the factors ϵJ_2^2, J_2^3, $J_2 J_\ell$ ($\ell > 2$), etc., plus cross coupling terms between short period fluctuations involving J_2 and those involving the lunar-solar effects. The long period fluctuations up to second order, obtained by integrating the long period rates (accurate to third order), are valid away from tesseral resonance and critical inclination.

B. DISTURBING FORCES

A study of the evolution of the orbit of a near-earth satellite valie for geodetic purposes requires that one account for all the disturbing forces that are likely to affect its motion. Ther zero order force is the central portion of the field of the earth, μ/r^2.

The first order disturbing force includes only the leading zonal harmonic J_2. The second order (in J_2) perturbing forces involve all the remaining zonal and tesseral harmonics, as well as the lunar and solar effects. The third order effects involve less-well-understood physical phenomena. These include ocean and land tides (physical deformation of the earth due to the lunar-solar gravitational forces acting on the earth), polar wandering, parallax effects of the lunar disturbing force, etc. As most of these third order effects (except the last) are not accurately known, their effects can be at most qualitatively described and will not be considered in this paper. For a discussion of the effects of tidal forces on satellite motion, the reader is referred to a paper by Kozai [11].

A second order theory will be presented here. The short period terms are given to second order in J_2. As the solution is to be valid for an extended period of time (10^3 rev), the long period and secular rates are computed to third order in J_2.

It is possible to carry artificial satellite theory beyond second order. Deprit [12] has carried the solution to third order in J_2 for the short period terms and to fourth order in J_2 for the secular terms. However, only the leading zonal harmonic J_2 was carried in his disturbing function.

C. CHOICE OF VARIABLES

Since only near circular orbits are considered, the use of Keplerian variables is undesirable. This is especially true in the case of M and ω, both of which lose their definition near $e = 0$. A more suitable set is $a, i, \xi, \eta, \Omega, u$ where $\xi = e \cos \omega$, $\eta = e \sin \omega$, $u = M + \omega$. The usual meaning is given to a, i, Ω. In the case of near zero inclinations, another variable change [13] is in order. However, an equatorial orbit is of limited use for geodetic purposes and will not be considered in this report.

D. THE DISTURBING FUNCTION

The disturbing function for a satellite in an earth orbit may be expressed as follows

$$F(a,i,\xi,\eta,u,\Omega) = R_e + R_M + R_s \tag{2.1}$$

where R_e is the terrestrial component of the disturbing function, and R_M and R_s denote the portions due to the moon and sun respectively. R_e, R_M, and R_s are expressed in terms of the orbital elements by the expressions

$$R_E = \frac{\mu}{r} \sum_{\ell=2}^{\infty} \sum_{m=0}^{\ell} J_{\ell m} \left(\frac{R}{r}\right)^{\ell} P_{\ell}^{m}(\sin \delta) \cos m(\varphi - \varphi_{\ell m}) \tag{2.2}$$

$$R_M = \frac{\mu_M r^2}{2r_M^3} \left[3\left(\frac{\bar{r}\cdot\bar{r}_M}{r r_M}\right)^2 - 1 \right] \tag{2.3}$$

$$R_s = \frac{\mu_s r^2}{2r_s^3} \left[3\left(\frac{\bar{r}\cdot\bar{r}_s}{r r_s}\right)^2 - 1 \right] \tag{2.4}$$

R_E is expanded to second order in ϵ and is expressed in terms of ξ and η as

$$R_E = \frac{\mu}{a} \sum_{\ell} \sum_{m} \sum_{p} \left(\frac{R}{a}\right)^{\ell} J_{\ell m} F_{\ell m p}(i)$$

$$\left[1 + Q_{\ell p o}(\xi^2 + \eta^2)\right] C_{\ell-2p,m}(u,\Omega,\theta_E)$$

$$Q_{\ell,p,+1}\left[\xi C_{\ell-2p+1,m} + \eta S_{(\ell-2p+1),m}\right]$$

$$Q_{\ell,p,-1}\left[\xi C_{\ell-2p-1,m} - \eta S_{\ell-2p-1,m}\right]$$

$$Q_{\ell,p,+2}\left[(\xi^2 - \eta^2) C_{\ell-2p+2,m} + 2\xi\eta S_{\ell-2p+2,m}\right]$$

$$Q_{\ell,p,-2}\left[(\xi^2 - \eta^2) C_{\ell-2p-2,m} - 2\xi\eta S_{\ell-2p-2,m}\right]$$

where

$$Q_{\ell po} = \left[\frac{\ell(\ell+1)}{4} - (\ell-2p)^2\right]$$

$$Q_{\ell,p,+1} = \left[\frac{\ell+1}{2} + \ell - 2p\right]$$

$$Q_{\ell,p,-1} = \left[\frac{\ell+1}{2} - (\ell-2p)\right]$$

$$Q_{\ell,p,+2} = \left(\frac{\ell+1}{2}\right)\left(\frac{\ell}{4}+1\right) + \left(\ell-2p\right)\left(\frac{9}{8}+\ell-p\right)$$

$$Q_{\ell,p,-2} = \left(\frac{\ell+1}{2}\right)\left(\frac{\ell}{4}+1\right) - \left(\ell-2p\right)\left(\frac{9}{8}+p\right)$$

and

$$C_{(\ell-2p),m}(u,\Omega,\theta_E) = \cos\left((\ell-2p)u + m(\Omega-\theta_E-\Phi_{\ell m}) + \psi_{\ell m}\right)$$

$$S_{(\ell-2p),m}(u,\Omega,\theta_E) = \sin\left((\ell-2p)u + m(\Omega-\theta_E-\Phi_{\ell m}) + \psi_{\ell m}\right)$$

$$\psi_{\ell m} = \begin{cases} 0 & (\ell-m) \text{ even} \\ \pi/2 & (\ell-m) \text{ odd} \end{cases}$$

$$F_{\ell mp}(i)^4 = \frac{(\ell+m)!}{2^\ell p!(\ell-p)!}\sum_k (-1)^k \binom{2\ell-2p}{k} \times \binom{2p}{\ell-m-k} \cos\left(\frac{i}{2}\right)^{3\ell-m-2p-2k} \times \sin\left(\frac{i}{2}\right)^{m-\ell+2p+2k} .$$

where the summation of k is from $k = \max(0, \ell-m-2p)$ to $k = \min(\ell-m,\ 2\ell-2p)$; $C_{\ell m}$ and $S_{\ell m}$ are related to $J_{\ell m}$ and $\varphi_{\ell m}$ by

$$C_{\ell m} = J_{\ell m} \cos\ (m\varphi_{\ell m})$$

$$S_{\ell m} = J_{\ell m} \sin\ (m\varphi_{\ell m})$$

The lunar portion of F is computed from Eq. 2.3. It is expanded to second order in ϵ_M and ϵ and is written as

$$\begin{aligned} R_m = \frac{\mu_m a^2}{2r_m^3\left(1-\epsilon_M^2\right)^{3/2}} \sum_p \sum_m \sum_n \sum_q A_{nq}\, R_{pmn}(i, I_M)^* \\ \Big\{ C_{(2-2p),m,n,q} \\ + (1-2p)\left[\xi\, C_{(2-2p+1),m,n,q} + \eta\, S_{(2-2p+1),m,n,q}\right] \\ - (3-2p)\left[\xi\, C_{(2-2p-1),m,n,q} - \eta\, S_{(2-2p-1),m,n,q}\right] \\ + \left[\frac{3}{2} - (2-2p)^2\right](\xi^2+\eta^2)\, C_{(2-2p),m,n,q} \\ + \left[\left(2-2p\right)\left(\frac{5}{8}-p\right) - \frac{1}{4}\right]\Big[(\xi^2-\eta^2)\, C_{(2-2p+2),m,n,q} \\ + 2\xi\eta\, S_{(2-2p+2),m,n,q}\Big] \\ + \left[\left(2-2p\right)\left(\frac{11}{8}-p\right) - \frac{1}{4}\right]\Big[(\xi^2-\eta^2)\, C_{(2-2p-2),m,n,q} \\ - 2\xi\eta\, S_{(2-2p-2),m,n,q}\Big]\Big\} \end{aligned} \qquad (2.6)$$

where

$$C_{(2-2p),m,n,q}(u,\ell_M,\Omega,\Omega_M,\omega_M) = \cos[(2-2p)u+m(\Omega-\Omega_M) + (n+q)\ell_M+n\omega_M]$$

$$S_{(2-2p),m,n,q}(u,\ell_M,\Omega,\Omega_M,\omega_M) = \sin[(2-2p)u+m(\Omega-\Omega_M) + (n+q)\ell_M+n\omega_M] ,$$

where

$$p = 0,1$$
$$m = -2,-1,0,+1,+2$$
$$n = -2,0,+2$$
$$q = -2,-1,0,+1,+2$$
$$A_{n\pm2} = \epsilon_M^2\left[n^2 \pm \frac{17}{8}\, n\right]$$
$$A_{n\pm1} = \epsilon_M\left[\frac{3}{2} \pm n\right]$$
$$A_{n,o} = 1 - 2n^2\epsilon_M^2 .$$

The solar portion of F is given by the same above expressions with

$$\mu_M \rightarrow \mu_s$$
$$r_M \rightarrow r_s$$
$$\omega_M \rightarrow \omega_s$$
$$I_M \rightarrow I_s$$
$$\Omega_M \rightarrow \Omega_s = 0$$
$$\ell_M \rightarrow \ell_s$$

The elements of the array $R_{pmn}(i, I_M)$ are given by

$$
\begin{aligned}
R_{0,-2,-2} &= \left[-\frac{3}{32} \sin^2 I_M + \frac{3}{8} \sin^2 (I_M/2) \right] (1-\cos i)^2 \\
R_{0,-2,0} &= \frac{3}{16} \sin^2 I_M (1-\cos i)^2 \\
R_{0,-2,+2} &= \frac{3}{8} \left[1 - \frac{1}{4} \sin^2 I_M - \sin^2 (I_M/2) \right] (1-\cos i)^2 \\
R_{0,-1,-2} &= \frac{3}{4} \sin I_M \sin^2 (I_M/2) \sin i (1-\cos i) \\
R_{0,-1,0} &= \left[\frac{3}{4} \sin I_M - \frac{3}{2} \sin I_M \sin^2 I_M/2 \right] \sin i (1-\cos i) \\
R_{0,-1,+2} &= \left[-\frac{3}{4} \sin I_M + \frac{3}{4} \sin I_M \sin^2 I_M/2 \right] \sin i (1-\cos i) \\
R_{0,0,-2} &= \frac{9}{16} \sin^2 I_M \sin^2 i \\
R_{0,0,0} &= \frac{3}{4} \left[1 - \frac{3}{2} \sin^2 I_M \right] \sin^2 i \\
R_{0,0,+2} &= \frac{9}{16} \sin^2 I_M \sin^2 i \\
R_{0,+1,-2} &= \frac{3}{4} \sin I_M (1-\sin^2 I_M/2) \sin i (1+\cos i) \\
R_{0,+1,0} &= -\frac{3}{4} \sin I_M (1-2 \sin^2 I_M/2) \sin i (1+\cos i) \\
R_{0,+1,+2} &= -\frac{3}{4} \sin I_M \sin^2 (I_M/2) \sin i (1+\cos i) \\
R_{0,+2,-2} &= \frac{3}{8} \left[1 - \frac{1}{4} \sin^2 I_M - \sin^2 (I_M/2) \right] (1+\cos i)^2 \\
R_{0,+2,0} &= \frac{3}{16} \sin I_M (1+\cos i)^2 \\
R_{0,+2,+2} &= \left[-\frac{3}{32} \sin^2 I_M + \frac{3}{8} \sin^2 (I_M/2) \right] (1+\cos i)^2
\end{aligned}
\tag{2.7}
$$

$$R_{1,-2,-2} = 0$$

$$R_{1,-2,0} = 0$$

$$R_{1,-2,+2} = 0$$

$$R_{1,-1,-2} = 0$$

$$R_{1,-1,0} = 0$$

$$R_{1,-1,+2} = 0$$

$$R_{1,0,-2} = 0$$

(2.7) cont

$$R_{1,0,0} = \frac{1}{4}\left[(3\cos^2 i - 1)(1 - \frac{3}{2}\sin^2 I_M)\right]$$

$$R_{1,0,+2} = \frac{1}{8}\sin^2 I_M(9\cos^2 i - 3)$$

$$R_{1,+1,-2} = -\frac{3}{2}\sin I_M(1 - \sin^2 I_M/2)\sin i \cos i$$

$$R_{1,1,0} = \frac{3}{2}\sin I_M(1 - 2\sin^2 I_M/2)\sin i \cos i$$

$$R_{1,1,+2} = \frac{3}{2}\sin I_M \sin^2(I_M/2)\sin i \cos i$$

$$R_{1,+2,-2} = \frac{3}{4}\left[1 - \frac{1}{4}\sin^2 I_M - \sin^2(I_M/2)\right]\sin^2 i$$

$$R_{1,+2,0} = \frac{3}{8}\sin^2 I_M \sin^2 i$$

$$R_{1,+2,+2} = \left[-\frac{3}{16}\sin^2 I_M + \frac{3}{4}\sin^2(I_M/2)\right]\sin^2 i$$

E. METHOD OF SOLUTION

The intrack, cross-track, and radial position fluctuations are determined with respect to a moving frame of reference defined by the mean orbital elements whose secular and long period rates are to be determined to third order. The short period radial and cross-track fluctuations due to J_2 and J_2^2 were obtained in a paper by Petty and Breakwell [Ref. 14]. There the position fluctuations with respect to the slowly moving frame of reference were determined directly. The orbit position as measured from the mean node was taken as the independent variable. The intrack fluctuations can thus be determined also to second order by the solution to the time equation. The computation of the long period and secular rates of the mean elements due to J_2 is carried out by the same method as outlined in Ref. 14.

Since only the first three leading zonal harmonics were included in this paper, the inclusion of the general zonal and tesseral harmonics, as well as the lunar-solar effects, would render the theory more complete. These effects are included but are obtained by application of the Lagrangian planetary equations. The short period intrack, cross-track, and radial position fluctuations, as well as the long period rates due to the additional terms, are determined directly. The tesseral harmonics contribute to no long period effects except at resonance, in which case a commensurability exists between the earth rotation and the satellite's mean motion. The interaction between the short period fluctuations due to J_2 and those resulting from J_ℓ ($\ell > 2$) and lunar-solar effects, also contribute to the long period and secular rates. These effects are also obtained by application of the Lagrangian planetary equations.

F. THE LAGRANGIAN PLANETARY EQUATIONS

The Lagrangian Planetary Equations can be written in terms of ξ, η and u. For small eccentricity, these equations are

$$\frac{da}{dt} = \frac{2}{na}\frac{\partial F}{\partial u}$$

$$\frac{d\Omega}{dt} = \frac{1}{na^2 \sin i}\frac{\partial F}{\partial i}$$

$$\frac{d\eta}{dt} = \frac{1}{na^2}\frac{\partial F}{\partial \xi} - \frac{\xi}{na^2}\frac{\cos i}{\sin i}\frac{\partial F}{\partial i}$$

$$\frac{d\xi}{dt} = -\frac{1}{na^2}\frac{\partial F}{\partial \eta} + \frac{\eta}{na^2}\frac{\cos i}{\sin i}\frac{\partial F}{\partial i}$$

$$\frac{di}{dt} = \frac{1}{na^2}\frac{\cos i}{\sin i}\frac{\partial F}{\partial u} - \frac{1}{na^2 \sin i}\frac{\partial F}{\partial \Omega} + \frac{1}{na^2}\frac{\cos i}{\sin i}\left(\xi\frac{\partial F}{\partial \eta} - \eta\frac{\partial F}{\partial \xi}\right) \qquad (2.8)$$

$$\frac{du}{dt} = -\frac{1}{na^2}\frac{\cos i}{\sin i}\frac{\partial F}{\partial i} - \frac{2}{na}\frac{\partial F}{\partial a} + \frac{1}{na^2}\left(\xi\frac{\partial F}{\partial \xi} - \eta\frac{\partial F}{\partial \eta}\right)$$

$$\overset{\circ}{h} = \frac{\partial F}{\partial u} + \xi\frac{\partial F}{\partial \eta} - \eta\frac{\partial F}{\partial \xi}$$

G. THE SHORT PERIOD TERMS

The radial, intrack, and cross-track fluctuations due to the second order part of the disturbing function (J_2 excluded), are determined from the relations

$$\delta r = \delta a + [\xi \sin u - \eta \cos u]a\delta u - a \cos u\delta\xi - a \sin u\delta\eta \qquad (2.9)$$

$$\delta\beta = \delta u + \cos i\ \delta\Omega + [2\xi \cos u + 2\eta \sin u]\delta u + 2\delta\xi \sin u - 2\delta\eta \cos u \qquad (2.10)$$

$$\delta\sigma = a \sin u\ \delta i - a \sin i \cos u\delta\Omega \quad . \qquad (2.11)$$

Equation 2.9 becomes

$$\left(\frac{\delta r}{a}\right) = \sum_{\ell} \sum_{m} \sum_{p} \left(\frac{R_0}{a}\right)^{\ell} F_{\ell mp}(i)$$

$$\times \left[\frac{2\ell - 4p}{\ell - 2p + m\lambda'} - \frac{\ell - 2p + \frac{\ell+1}{2}}{\ell - 2p + 1 + m\lambda'} - \frac{\ell - 2p - \frac{\ell+1}{2}}{\ell - 2p - 1 + m\lambda'} \right] J_{\ell m}$$

$$\times \cos\left[(\ell-2p)u + m(\Omega - \theta_E - \varphi_{\ell m}) + \psi_{\ell m}\right]$$

$$+ \frac{1}{2} \frac{\left(\mu_s / r_s^3\right)}{(\mu/a^3)} \sum_{p} \sum_{m} \sum_{n} R_{pmn}(i, I_s)$$

$$\times \left[\frac{4 - 4p}{(2-2p)(1+\omega') + \lambda'_{mns}} - \frac{1 - 2p}{(2-2p)\omega' + (2-2p+1) + \lambda'_{mns}} \right.$$

$$\left. - \frac{3 - 2p}{(2-2p)\omega' + (2-2p-1) + \lambda'_{mns}} \right] \qquad (2.12)$$

$$\times \cos\left[(2 - 2p)u + m\Omega + n(\ell_s + \omega_s)\right]$$

$$+ \frac{1}{2} \frac{\left(\mu_m / r_m^3\right)}{\mu/a^3} \sum_{p} \sum_{m} \sum_{n} R_{pmn}(i, I_m)$$

$$\times \left[\frac{4 - 4p}{(2-2p)(1+\omega') + \lambda'_{mnm}} - \frac{1 - 2p}{(2-2p)\omega' + (2-2p+1) + \lambda'_{mnm}} \right.$$

$$\left. - \frac{3 - 2p}{(2-2p)\omega' + (2-2p+1) + \lambda'_{mnm}} \right]$$

$$\times \cos\left[(2-2p)u + m(\Omega-\Omega_M) + n(\ell_M + \omega_M)\right]$$

where $p = 0$, $m = -2, -1, 0, +1, +2$, $n = -2, 0, +2$ in the lunar and solar contribution.

Equation 2.10 becomes

$$\frac{\delta\beta}{a} = \sum_{\ell}\sum_{m}\sum_{p}\left(\frac{R_0}{a}\right)^{\ell} F_{\ell mp}(i)$$

$$\times \left[\frac{2\ell + 2}{\ell-2p+m\lambda'} - \frac{3\ell - 4p + 1}{\ell-2p+1+m\lambda'} + \frac{\ell - 2p - 1}{\ell-2p-1+m\lambda'} - \frac{3(\ell - 2p)}{(\ell-2p+m\lambda')^2}\right]$$

$$\times \sin\left[(\ell-2p)u + m(\Omega-\theta_E - \varphi_{\ell m}) + \psi_{\ell m}\right] \qquad (2.13)$$

$$+ \frac{1}{2}\frac{\left(\mu_s/r_s^3\right)}{(\mu/a^3)} \sum_{p}\sum_{m}\sum_{n} R_{pmn}(i,Is)\left[\frac{-4}{(2-2p)(\omega'+1)+\lambda'_{mns}}\right.$$

$$- \frac{(2 - 4p)}{(2-2p)\omega'+(2-2p+1)+\lambda'_{mns}}$$

$$\left. + \frac{6 - 4p}{(2-2p)\omega'+(2-2p-1)+\lambda'_{mns}} - \frac{(6 - 6p)}{\left[(2-2p)(\omega'+1)+\lambda'_{mns}\right]^2}\right]$$

$$\times \sin\left[(2-2p)u + m\Omega\ 2\ n(\ell_s + \omega_s)\right]$$

$$+ \frac{1}{2} \frac{\left(\mu_M / r_M^3\right)}{\left(\mu / a^3\right)} \sum_p \sum_m \sum_n R_{pmn}(i, Im)$$

$$\times \left[\frac{-4}{(2-2p)(\omega'+1)+\lambda'_{mnM}} - \frac{-(2-4p)}{2-2p)\omega'+(2-2p+1)+\lambda'_{mnM}} \right. \qquad (2.13)$$

$$\left. + \frac{6-4p}{(2-2p)\omega'+(2-2p-1)+\lambda'_{mnM}} - \frac{-(6-6p)}{\left[(2-2p)(\omega'+1)+\lambda'_{mnM}\right]^2} \right]$$

$$\times \sin\left[(2-2p)u + m(\Omega - \Omega_M) + n(\ell_M + \omega_M)\right]$$

Equation 2.11 becomes

$$\frac{\delta\sigma}{a} = \frac{1}{2} \sum_\ell \sum_m \sum_p J_{\ell m} \left(\frac{R_0}{a}\right)^\ell \frac{d\, F_{\ell mp}(i)}{di} \frac{1}{\left[(\ell-2p)(1+\omega\ )+m\lambda'\right]}$$

$$\times \left\{ \sin\left[(\ell - 2p + 1)u + m(\Omega - \theta_E - \varphi_{\ell m}) + \psi_{\ell m}\right] \right.$$

$$\left. + \sin\left[(\ell - 2p - 1)u + m(\Omega - \theta_E - \varphi_{\ell m}) + \psi_{\ell m}\right] \right\} \qquad (2.14)$$

$$+ \frac{1}{2} \sum_\ell \sum_m \sum_p J_{\ell m} \left(\frac{R_0}{a}\right)^\ell \frac{F_{\ell mp}(i)}{\sin(i)} \left[\frac{(\ell-2p)\cos i - m}{(\ell-2p)(\omega'+1)+m\lambda'}\right]$$

$$\times \left\{ \sin\left[(\ell - 2p + 1)u + m(\Omega - \theta_E - \varphi_{\ell m}) + \psi_{\ell m}\right] \right.$$

$$\left. - \sin\left[(\ell - 2p - 1)u + m(\Omega - \theta_E - \varphi_{\ell m}) + \psi_{\ell m}\right] \right\}$$

$$- \frac{1}{4} \frac{\left(\mu_s / r_s^3\right)}{(\mu / a^3)} \sum_p \sum_m \sum_n \left[\frac{d\, R_{pmn}(i)/di}{(2-2p)(\omega'+1) + \lambda'_{mns}} \right]$$

$$\times \quad \sin\left[(3 - 2p)u + m\Omega + n(\ell_s + \omega_s)\right]$$
$$\sin\left[(1 - 2p)u + m\Omega + n(\ell_s + \omega_s)\right]$$

$$+ \frac{1}{4}\frac{\left(\mu_s/r_s^3\right)}{(\mu/a^3)} \sum_p \sum_m \sum_n \frac{R_{pmn}(i)}{\sin i}\left[\frac{(2-2p)\cos i - m}{(2-2p)(\omega'+1)+\lambda'_{mns}}\right]$$

$$\times \left\{ \sin\left[(3 - 2p)u + m\Omega + n(\ell_s + \omega_s)\right] \right.$$
$$\left. - \sin\left[(1 - 2p)u + m\Omega + n(\ell_s + \omega_s)\right]\right\} \qquad (2.14)\ \text{cont}$$

$$- \frac{1}{4}\frac{\left(\mu_m/r_m^3\right)}{(\mu/a^3)} \sum_p \sum_m \sum_n \frac{d\, R_{pmn}(i)/di}{(2-2p)(\omega'+1)+\lambda'_{mnM}}$$

$$\times \left\{ \sin\left[(3 - 2p)u + m(\Omega - \Omega_M) + n(\ell_M + \omega_M)\right] \right.$$
$$\left. + \sin\left[(1 - 2p)u + m(\Omega - \Omega_M) + n(\ell_M + \omega_M)\right]\right\}$$

$$+ \frac{1}{4}\frac{\left(\mu_m/r_m^3\right)}{(\mu/a^3)} \sum_p \sum_m \sum_n \frac{R_{pmn}(i)}{\sin i}\left[\frac{(2 - 2p)\cos i - m}{(2-2p)(\omega +1)+\lambda_{mnM}}\right]$$

$$\times \left\{ \sin\left[(3 - 2p)u + m(\Omega - \Omega_M) + n(\ell_M + \omega_M)\right] \right.$$
$$\left. - \sin\left[(1 - 2p)u + m(\Omega - \Omega_M) + n(\ell_M + \omega_M)\right]\right\}$$

where

$$\theta_E = \omega_0 t$$

ω_0 = angular rate of earth rotation

$$\lambda' = -\frac{\omega_0 + \dot{\Omega}}{\dot{\bar{f}}}$$

$$\lambda'_{mns} = \frac{m\dot{\Omega} + n\dot{\theta}_s}{\dot{\bar{f}}}$$

$$\lambda'_{mnM} = \frac{m\dot{\Omega} + n\dot{\theta}_m}{\dot{\bar{f}}}$$

$$\omega' = \frac{d\omega}{d}$$

$$\theta_s = \ell_s + \omega_s$$

$$\theta_M = \ell_M + \omega_M \ .$$

The short period radial and cross-track position fluctuations due to J_2 and J_2^2 are determined in a paper by Petty and Breakwell [Ref. 14]. Here, a noncanonical approach is followed with orbit position taken as the independent variable. Only the leading zonal harmonics J_2, J_3, and J_4 are kept in the equations of motion. The short period fluctuations are determined with respect to a slowly rotating frame of reference. The intrack fluctuations are determined by the solution to the time equation.

The radial and out-of-plane fluctuations are given to second order in J_2 as

$$\begin{aligned}\rho = \frac{1}{r} = \frac{\mu}{h^2}\Big[&1 + \xi \cos u' + \eta \sin u' + \bar{J}_2\left(1 - \frac{3}{2}\sin^2 i\right) \\ &+ \bar{J}_2^2\left(2 - \frac{13}{2}\sin^2 i + \frac{109}{24}\sin^4 i\right) - \frac{\bar{J}_2}{6}\sin^2 i \cos 2U' \\ &+ \frac{\bar{J}_2^2}{9}\sin^2 i(2 - \sin^2 i)\cos 2U' \\ &- \frac{5}{24}\bar{J}_2 \sin^2 i(\xi \cos 3U' + \eta \sin 3U') \\ &+ \frac{J_2^2}{24}\sin^2 i \cos 4U'\Big]\end{aligned}$$

$$\begin{aligned}\sigma = &- \bar{J}_2 \sin i \cos i \, \eta \\ &+ \frac{1}{3}\bar{J}_2 \sin i \cos i(\xi \sin 2U' - \eta \cos 2U') \\ &- \frac{5}{24}\bar{J}_2^2 \sin^3 i \cos i \sin 3U' \ .\end{aligned}$$

H. THE TIME EQUATION

Since the orbit position U' is being used as the independent variable, its relationship to time is desired if the intrack position fluctuations are desired. The time equation is carried to order $\bar{J}_2\xi^2$ and $J_\ell\eta$ where $\ell = 3,5,7,\ldots$ terms containing J_2^3, J_2J_ℓ are dropped as these are indistinguishable from a slight adjustment of the mean semi-major axis a. The time equation is written as

$$
\begin{aligned}
\frac{dt}{dU'} = \frac{1}{n}\left[1 + \cos i \frac{d\Omega}{dU'}\right]\Bigg\{ & 1 - 2\xi\cos U' - 2\eta \sin U' \\
& - 2\bar{J}_2\left(1 - \frac{3}{2}\sin^2 i\right) - \frac{1}{6}\bar{J}_2 \sin^2 i \cos 2U' \\
& + \frac{3}{2}(\xi^2 + \eta^2) + \frac{3}{2}(\xi^2 - \eta^2)\cos 2U' \\
& + 3\eta\xi \sin 2U' + 6\bar{J}_2(\xi\cos U' + \eta \sin U') \\
& - \bar{J}_2^2 + \frac{1}{4}\bar{J}_2 \sin^2 i(\xi \cos 3u + \eta \sin 3U') \\
& - \frac{19}{2}\bar{J}_2 \sin^2 i\, \xi \cos U' - \frac{51}{6}\bar{J}_2 \sin^2 i\, \eta \sin U' \\
& + 4\bar{J}_2^2 \sin^2 i - \frac{25}{36}\bar{J}_2^2 \sin^2 i \cos 2U' \\
& - \frac{9}{4}\bar{J}_2^2 \sin^4 i + \frac{1}{12}\bar{J}_2^2 \sin^2 i \cos 4U' \\
& + \frac{13}{18}\bar{J}_2^2 \sin^2 i \cos 2U' + \frac{3}{4}\bar{J}_2 \xi^2 \sin^2 i \\
& + \frac{1}{n}\sum_{\ell,m,p} J_{\ell m}\left(\frac{R}{a}\right)^\ell \left[\frac{\cos i}{\sin i}\frac{\partial F_{\ell,m,p}(i)}{\partial i} - 2(\ell+1)F_{\ell,m,p}(i)\right] \\
& \qquad \times \cos\left[(\ell - 2p)U' + m(\Omega - \theta_E - \varphi_{\ell m}) + \psi_{\ell m}\right] \\
& + \frac{\mu_M/r_M^3}{n^3}\sum_{m,n,p}\left[\frac{1}{2}\frac{\cos i}{\sin i}\frac{\partial R_{p,m,n}(i, I_M)}{\partial i} + 4R_{p,m,n}\right] \\
& \qquad \times \cos\left[(2 - 2p)U' + m(\Omega - \Omega_M) + n(\ell_M + \omega_M)\right]
\end{aligned}
\tag{2.17}
$$

$$+ \frac{\mu_s/r_s^3}{n^3} \sum_{m,n,p} \left[\frac{1}{2} \frac{\cos i}{\sin i} \frac{\partial R_{p,m,n}(i_1 I_s)}{\partial i} + 4 R_{p,m,n} \right]$$

$$\times \cos \left[(2 - 2p)U' + m\Omega + n(\ell_s + \omega_s) \right] \qquad (2.17)\ \text{cont}$$

$$+ \frac{1}{n} \sum_{\ell=3,5,7,\ldots} J_\ell \left(\frac{R}{a}\right)^\ell \eta \left[\frac{\cos i}{\sin i} \frac{\partial}{\partial i} \left(F_{\ell,o,(\ell+1)/2} - F_{\ell,o,(\ell-1/2)} \right) \right.$$

$$\left. - 2(\ell+1) \left(F_{\ell,o,(\ell+1)/2} - F_{\ell,o,(\ell-1/2)} \right) \right]$$

$$+ \frac{1}{n} \sum_{\ell=3,5,7} J_\ell \left(\frac{R}{a}\right)^\ell \eta \left(\frac{\ell-1}{2}\right) \left[\frac{\cos i}{\sin i} \frac{\partial}{\partial i} \left(F_{\ell,o,(\ell+1)/2} - F_{\ell,o,(\ell-1)/2} \right) \right.$$

$$\left. - 2(\ell+1) \left(F_{\ell,o,(\ell+1)/2} - F_{\ell,o,(\ell-1)/2} \right) \right]$$

$$- \frac{1}{n} \sum_{\ell=3,5,7} J_\ell \left(\frac{R}{a}\right)^\ell \eta \left(\frac{\ell-1}{2}\right) \left(F_{\ell,o,(\ell+1)/2} - F_{\ell,o,(\ell-1)/2} \right)$$

9. THE LONG PERIOD AND SECULAR RATES

In order to achieve a complete second order theory, the long period and secular rates must be determined to third order in J_2 and mean eccentricity. When applying Lagrange's planetary equations to the disturbing function (Eqs. 2.5 and 2.6, the resulting expression contains secular, long period (periodic in Ω and ω), and short period terms periodic in the mean anomaly. To obtain the mean rates of the elements, it is not sufficient to average the short period terms out when higher order terms are involved. The short period terms are functions of the instantaneous elements which themselves contain short period fluctuations. These couple with the short period terms to produce higher order contributions to the long period and secular rates of the elements. The resulting expressions are functions of the mean elements and should not be confused with the instantaneous elements. The secular and long period rates of the mean elements are given in terms of the mean elements as

$$\frac{di}{dU'} = \sum_{\ell=3,5,7,\ldots} J_\ell \left(\frac{R}{a}\right)^\ell \left(\frac{\ell-1}{2}\right) \frac{\cos i}{\sin i} \xi \left(F_{\ell,o,(\ell+1)/2} - F_{\ell,o,(\ell-1)/2}\right)$$

$$+ \frac{\mu_s/r_s^3}{\mu/a^3} \frac{1}{(1-\epsilon_s^2)^{\frac{3}{2}}} \sum_{m,n,q} A_{nq} R_{lmn}(i, I_s) \frac{m}{\sin i}$$

$$\times \sin[m\Omega + (n+q)\ell_s + n\omega_s]$$

$$+ \frac{\mu_M/r_M^3}{\mu/a^3} \frac{1}{(1-\epsilon_M^2)^{\frac{3}{2}}} \sum_{m,n,q} A_{nq} R_{lmn}(i, I_M) \frac{m}{\sin i}$$

$$\times \sin[m(\Omega - \Omega_M) + (n+q)\ell_M + n\omega_M] \; ; \qquad (2.18)$$

$$\frac{1}{h}\frac{dh}{dU'} = \sum_{\ell=3,5,7,\ldots} J_\ell \left(\frac{R}{a}\right)^\ell \left(\frac{\ell-1}{2}\right) \xi \left[F_{\ell,o,(\ell+1)/2} - F_{\ell,o,(\ell-1)/2}\right]; \qquad (2.19)$$

$$\frac{d\Omega}{dU'} = -\bar{J}_2 \cos i + \frac{1}{2}\bar{J}_2^2 \cos i \left(1 - \frac{2}{3}\sin^2 i\right)$$

$$-\bar{J}_2^3 \cos i \left(\frac{3}{2} - \frac{175}{36}\sin^2 i + \frac{235}{72}\sin^4 i\right)$$

$$+ \sum_{\ell=4,6,8,\ldots} J_\ell \left(\frac{R}{a}\right)^\ell \frac{1}{\sin i} \frac{\partial F_{\ell,o,\ell/2}}{\partial i} \qquad (2.20)$$

$$+ \sum_{\ell=3,5,7,\ldots} J_\ell \left(\frac{R}{a}\right)^\ell \left(\frac{\ell-1}{2}\right) \frac{\eta}{\sin i} \frac{\partial}{\partial i} \left(F_{\ell,o,(\ell+1)/2} - F_{\ell,o,(\ell-1)/2}\right)$$

$$+ \sum_{\ell=4,6,8,\ldots} J_2 J_\ell \left(\frac{R}{a}\right)^{\ell+2} \Bigg\{ -\frac{1}{12} \sin i \frac{\partial}{\partial i} \left(F_{\ell,o,(\ell+2)/2} + F_{\ell,o,(\ell-2)/2}\right)$$

$$- \frac{1}{\sin i}\left(3 - 4\sin^2 i\right) \frac{\partial F_{\ell,o,\ell/2}}{\partial i}$$

$$-\left(\frac{3}{4}\ell + \frac{9}{8}\right) \sin i \frac{\partial}{\partial i} \left(F_{\ell,o,(\ell+2)/2} + F_{\ell,o,(\ell-2)/2}\right)$$

$$
- \frac{3}{8} \cos i \frac{\partial^2}{\partial i^2}\left(F_{\ell,o,(\ell+2)/2} + F_{\ell,o,(\ell-2)/2}\right)
$$

$$
+ \frac{3}{8} \frac{\cos^2 i}{\sin i} \frac{\partial}{\partial i}\left(F_{\ell,o,(\ell+2)/2} + F_{\ell,o,(\ell-2)/2}\right)
$$

$$
\left(\frac{9}{4} - 3\cos^2 i\right) \frac{1}{\sin i} \frac{\partial}{\partial i}\left(F_{\ell,o,(\ell+2)/2} + F_{\ell,o,(\ell-2)/2}\right)\Bigg\}
$$

$$
+ \frac{1}{2} \frac{\mu_s/r_s^3}{\mu/a^3} \frac{1}{(1-\epsilon_s^2)^{\frac{3}{2}}} \sum_{m,n,q} A_{nq} \frac{1}{\sin i} \frac{\partial}{\partial i} R_{l,m,n}(i, I_s)
$$

$$
\cos[m\Omega + (n+q)\ell_s + n\omega_s]
$$

$$
\frac{1}{2} \frac{\mu_M/r_M^3}{\mu/a^3} \frac{1}{(1-\epsilon_M^2)^{\frac{3}{2}}} \sum_{m,n,q} A_{nq} \frac{1}{\sin i} \frac{\partial}{\partial i} R_{l,m,n}(i, I_m)
$$

$$
\cos[m(\Omega-\Omega_M) + (n+q)\ell_M + n\omega_M]
$$

$$
+ \frac{3}{16} \frac{\mu_M/r_M^3}{\mu/a^3} J_2\left(\frac{R}{a}\right)^2 \sum_{m,n} \Bigg[3 \sin i \frac{\partial R_{o,m,n}}{\partial i}(i, I_M)
$$

$$
- \cos i \frac{\partial^2}{\partial i^2} R_{o,m,n}(i, I_M) + \frac{\cos^2 i}{\sin i} \frac{\partial R_{o,m,n}}{\partial i}(i, I_M)
$$

$$
- \left(\frac{4\cos^2 i - 3}{\sin i}\right) \frac{\partial R_{o,m,n}}{\partial i}\Bigg] \cos[m(\Omega-\Omega_M) + n(\ell_M + \omega_M)]
$$

$$
+ \frac{3}{16} \frac{\mu_s/r_s^3}{\mu/a^3} J_2\left(\frac{R}{a}\right)^2 \sum_{m,n} \Bigg[3 \sin i \frac{\partial R_{o,m,n}}{\partial i}(i, I_s)
$$

$$
- \cos i \frac{\partial^2}{\partial i^2} R_{o,m,n}(i, I_s) + \frac{\cos^2 i}{\sin i} \frac{\partial}{\partial i} R_{o,m,n}(i, I_s)
$$

$$
- \left(\frac{4\cos^2 i - 3}{\sin i}\right) \frac{\partial R_{o,m,n}}{\partial i}\Bigg] \cos[m\Omega + n(\ell_s + \omega_s)]
$$

(2.20) cont

$$\frac{d\eta}{dU'} = 2\bar{J}_2\xi\left(1 - \frac{5}{4}\sin^2 i\right) - \bar{J}_2^2\,\xi\sin^2 i\left(\frac{9}{4}\sin^2 i - \frac{5}{2}\right)$$

$$+ \sum_{\ell=4,6,8,\ldots} J_\ell\left(\frac{R}{a}\right)^\ell \xi\left[\frac{\ell(\ell+1)}{2}F_{\ell,o,\ell/2} - \frac{\cos i}{\sin i}\frac{\partial F_{\ell,o,\ell/2}}{\partial i}\right]$$

$$+ \frac{\mu_M/r_M^3}{\mu/a^3}\sum_{m,n}\left\{\left[3R_{1,m,n}(i,I_M) - \frac{\cos i}{\sin i}\frac{\partial R_{1,m,n}}{\partial i}\right]\right.$$

$$\times \xi\cos[m(\Omega - \Omega_M) + n(\ell_M + \omega_M)]$$

$$+ 5R_{o,m,n}(i,I_M)\left(\xi\cos[m(\Omega-\Omega_M) + n(\ell_M + \omega_M)]\right. \qquad (2.21)$$

$$\left.\left. - \eta\sin[m(\Omega-\Omega_M) + n(\ell_M + \omega_M)]\right]\right\}$$

$$+ \frac{\mu_s/r_s^3}{\mu/a^3}\sum_{m,n}\left\{\left[3R_{1,m,n}(i,I_s) - \frac{\cos i}{\sin i}\frac{\partial R_{1,m,n}}{\partial i}\right]\right.$$

$$+ \xi\left[\cos m\Omega + n(\ell_s + \omega_s)\right]$$

$$+ 5\,R_{om,mn}(i,I_s)\left(\xi\cos\left[m\Omega + n(\ell_s + \omega_s)\right]\right.$$

$$\times \xi\cos\left[m\Omega + n(\ell_s + \omega_s)\right]$$

$$\left.\left. - \eta\sin\left[m\Omega + n(\ell_s + \omega_s)\right]\right)\right\}$$

$$\frac{d\xi}{dU'} = -2\bar{J}_2\eta\left(1 - \frac{5}{4}\sin^2 i\right) + \bar{J}_2^2\eta\left(\frac{1}{3}\sin^2 i + \frac{1}{4}\sin^2 i\right)$$

$$+ \sum_{\ell=4,6,8,..} J_\ell\left(\frac{R}{a}\right)^\ell \eta\left[-2F_{\ell,o,\ell/2}Q_{\ell,\ell/2,o}\right. \qquad (2.22)$$

$$+ 2F_{\ell,o,(\ell+2)/2}Q_{\ell,(\ell+2)/2,+2}$$

$$+ 2F_{\ell,o,(\ell-2)/2}Q_{\ell,(\ell-2)/2,-2}$$

$$\left. + \frac{\cos i}{\sin i}\frac{\partial F_{\ell,o,\ell/2}}{\partial i}\right]$$

$$+ \sum_{\ell=3,5,7,\ldots} J_\ell \left(\frac{R}{a}\right)^\ell \left(\frac{\ell - 1}{2}\right) \left[F_{\ell,o,(\ell-1)/2} - F_{\ell,o,(\ell+1)/2}\right]$$

$$\times \sum_{\ell=3,5,7,\ldots} J_2 J_\ell \left(\frac{R}{a}\right)^{\ell+2} \left[\left(\frac{21}{8}\sin^2 i - \frac{3}{2}\right)\left(F_{\ell,o,(\ell-1)/2} Q_{\ell,(\ell-1)/2,0} - F_{\ell,o,(\ell+1)/2} Q_{\ell,(\ell+1)/2,0}\right)\right]$$

$$- \frac{7}{8}\sin^2 i \left(F_{\ell,o,(\ell-3)/2} Q_{\ell,(\ell-3)/2,0} - F_{\ell,o,(\ell+3)/2} Q_{\ell,(\ell+3)/2,0}\right)$$

$$+ \left(\frac{3}{4}\ell + \frac{9}{8}\right)\sin^2 i \left(F_{\ell,o,(\ell-1)/2} Q_{\ell,(\ell-1)/2,+1} + F_{\ell,o,(\ell+3)/2} Q_{\ell,(\ell+3)/2,+1}\right)$$

$$+ \frac{3}{8}\sin i \cos i \left(F_{\ell,o,(\ell-1)/2} Q_{\ell,(\ell-1)/2,+1} + F_{\ell,o,(\ell+3)/2} Q_{\ell,(\ell+3)/2,+1}\right) \qquad (2.22)\ \text{cont.}$$

$$+ \left(3\cos^2 i - \frac{9}{4}\right)\left(F_{\ell,o,(\ell-1)/2} Q_{\ell,(\ell-1)/2,+1} - F_{\ell,o,(\ell+3)/2} Q_{\ell,(\ell+3)/2,+1}\right)$$

$$- \left(\frac{3}{4}\ell + \frac{9}{8}\right)\sin^2 i \left[F_{\ell,o,(\ell-3)/2} Q_{\ell,(\ell-3)/2,-1} + F_{\ell,o,(\ell+1)/2} Q_{\ell,(\ell+1)/2,-1}\right]$$

$$- \frac{3}{8}\sin i \cos i \left[F_{\ell,o,(\ell-3)/2} Q_{\ell,(\ell-3)/2,-1} + F_{\ell,o,(\ell+1)/2} Q_{\ell,(\ell+1)/2,-1}\right]$$

$$- \left(3\cos^2 i - \frac{9}{4}\right)\left[F_{\ell,o,(\ell-3)/2} Q_{\ell,(\ell-3)/2,-1} + F_{\ell,o,(\ell+1)/2} Q_{\ell,(\ell+1)/2,-1}\right]$$

$$- \left(\frac{21}{8}\sin^2 i - \frac{3}{2}\right)\left[F_{\ell,o,(\ell+1)/2} Q_{\ell,(\ell+1)/2,+2} - F_{\ell,o,(\ell+3)/2} Q_{\ell,(\ell+3)/2,+2}\right]$$

$$+ \frac{7}{8}\sin^2 i \left[F_{\ell,o,(\ell-1)/2} Q_{\ell,(\ell-1)/2,+2} - F_{\ell,o,(\ell+5/2} Q_{\ell,(\ell+5)/2,+2}\right]$$

$$+ \left(\frac{15}{8}\sin^2 i - \frac{3}{2}\right)\left[F_{\ell,o,(\ell+1)/2^Q\ell,(\ell+1)/2,+2} + F_{\ell,o,(\ell+3)/2^Q\ell,(\ell+3)/2,+2}\right]$$

$$- \frac{7}{8}\sin^2 i\left[F_{\ell,o,(\ell-1)/2^Q\ell,(\ell-1)/2,+2} + F_{\ell,o,(\ell+5)/2^Q\ell,(\ell+5)/2,2}\right]$$

$$- \left(\frac{21}{8}\sin^2 i - \frac{3}{2}\right)\left[F_{\ell,o,(\ell-3)/2^Q\ell,(\ell-3)/2,-2} - F_{\ell,o,(\ell-1)/2^Q\ell,(\ell-1)/2,-2}\right]$$

$$+ \frac{7}{8}\sin^2 i\left[F_{\ell,o,(\ell-5)/2^Q\ell,(\ell-5)/2,-2} - F_{\ell,o,(\ell+1)/2^Q\ell,(\ell+1)/2,-2}\right]$$

$$- \left(\frac{15}{8}\sin^2 i - \frac{3}{2}\right)\left[F_{\ell,o,(\ell-3)/2^Q\ell,(\ell-3)/2,-2} + F_{\ell,o,(\ell-1)/2^Q\ell,(\ell-1)/2,-2}\right]$$

$$+ \frac{7}{8}\sin^2 i\left[F_{\ell,o,(\ell-5)/2^Q\ell,(\ell-5)/2,-2} + F_{\ell,o,(\ell+1)/2^Q\ell,(\ell+1)/2,-2}\right]$$

$$- \left(\frac{21}{8}\sin^2 i - \frac{3}{2}\right)\left[\frac{\partial F_{\ell,o,(\ell-1)/2}}{\partial i} - \frac{\partial F_{\ell,o,(\ell+1)/2}}{\partial i}\right]$$

$$+ \frac{7}{8}\sin^2 i\left[\frac{\partial F_{\ell,o,(\ell-3)/2}}{\partial i} - \frac{\partial F_{\ell,o,(\ell+3)/2}}{\partial i}\right] \qquad \text{(2.22) cont}$$

$$+ \left(\frac{9}{2} - 6\sin^2 i\right)\left[F_{\ell,o,(\ell+1)/2^Q\ell,(\ell+1)/2,+1} - F_{\ell,o,(\ell-1)/2^Q\ell,(\ell-1)/2,+1}\right]$$

$$+ \frac{1}{12}\sin^2 i\left[F_{\ell,o,(\ell-1)/2^Q\ell,(\ell-1)/2,+1} + F_{\ell,o,(\ell+3)/2^Q\ell,(\ell+3)/2,+1}\right.$$

$$\left. - F_{\ell,o,(\ell-3)/2^Q\ell,(\ell-3)/2,-1} - F_{\ell,o,(\ell+1)/2^Q\ell,(\ell+1)/2,-1}\right]\Bigg\}$$

$$+ \sum_{\ell=4,6,8,\ldots} J_\ell\left(\frac{R}{a}\right)^\ell \eta\left[F_{\ell,o,(\ell/2)^Q\ell,(\ell/2),+1} - F_{\ell,o,(\ell+2)/2^Q\ell,(\ell+2)/2,+1}\right.$$

$$\left. - F_{\ell,o,(\ell-2)/2^Q\ell,(\ell-2)/2,-1} + F_{\ell,o,(\ell/2)^Q\ell,(\ell/2),-1}\right]$$

$$+ \frac{1}{2}\frac{\mu_s/r_s^3}{\mu/a^3}\sum_{m,n}\left\{\left[3R_{l,m,n}(i,I_s) - \frac{\cos i}{\sin i}\frac{\partial R_{l,m,n}}{\partial i}\right]\eta\cos\left[m\Omega + n(\ell_s + \omega_s)\right]\right.$$

$$\left. + 5R_{o,m,n}(i,I_s)\left(\eta\cos\left[m\Omega + n(\ell_s + \omega_s)\right] + \xi\sin\left[m\Omega + n(\ell_s + \omega_s)\right]\right)\right\}$$

$$+ \frac{1}{2}\frac{\mu_M/r_M^3}{\mu/a^3}\sum_{m,n}\left[3R_{l,m,n}(i,I_M) - \frac{\cos i}{\sin i}\frac{\partial R_{l,m,n}}{\partial i}\right]\eta\cos\left[m(\Omega-\Omega_M)+n(\ell_M+\omega_M)\right] \quad \text{cont} \quad (2.22)$$

$$\left. + 5R_{o,m,n}(i,I_M)\left(\eta\cos\left[m(\Omega-\Omega_M)+n(\ell_M+\omega_M)\right] + \xi\sin\left[m(\Omega-\Omega_M) + n(\ell_M + \omega_M)\right]\right)\right\}$$

J. CONCLUSIONS

The question comes up as to what type of position fluctuations arise as a result of the various disturbing forces. The following Table summarizes these results.

Disturbing Term	Frequency (inplane fluc/orbit)
J_2	2
ϵJ_2	2, 4
J_2^2	1, 3
$J_{\ell m}$	$\ell - 2p$ $(p = 0,1,\ldots\ell)$
$\epsilon J_{\ell m}$	$\ell - 2p \pm 1$
lunar solar terms (zero eccentricity)	2

Terms involving $\epsilon J_{\ell m}$ are not carried in the solution since an almost circular orbit is assumed. However, should the chosen orbit be slightly eccentric, one would expect to observe, for example, due to ϵJ_5 1,3,5 and 7, fluctuations per orbit. Should a frequency of ℓ fluctuations per orbit be observed, the contributing coefficients would be J_ℓ, $J_{\ell+2}$,... $J_{\ell+4}$,..., $\epsilon J_{\ell\pm1}$, $\epsilon J_{\ell\pm3}$, $\epsilon J_{\ell\pm5}$..., etc.

The solution as presented is capable of fitting the observed data for any time period. Alternatively, if the dynamical shape of the earth were known to at least 10^{-9}g, and the initial orbit were known to the required accuracy, the solution is capable of one meter accuracy over an extended period of time. As the solution is valid for a circular orbit, the number of terms required is greatly reduced from that required for an eccentric orbit. The solution is a purely literal form expressed in terms of the elementary functions. It can be easily implemented on a computer.

IV. SATELLITE DESIGN

A. PROOF MASS DISTURBANCES

1. Effect of Proof Mass Disturbances on the Orbit

Satellite disturbing forces do not have an equal effect in perturbing a satellite from its gravitational path for all directions in space. The relative effect on perturbations in different directions due to forces acting vertically, intrack, and normal to the orbit plane are shown for sinusoidal disturbances in Fig. IV-1. Forces acting normal to the orbit plane displace the orbit plane until the component of gravity, due to the displacement, equals the disturbing force. As long as the disturbances vary slowly compared to orbital frequency, assumed for each of the sketches in Fig. IV-1, the displacement is independent of time, and is an equilibrium displacement like a force acting against a spring. The same effect occurs for a vertical displacement due to a vertical force. These effects are shown quantitatively in the upper left-hand corner of Fig. IV-1. A vertical force changes the radius of the orbit but it also changes its period. This causes the satellite to change its position relative to the gravitational path at a constant rate and the displacement increases with time. Therefore, a sinusoidally varying vertical force produces a peak error intrack which depends upon the frequency of the disturbance. A similar effect is produced by intrack perturbing forces. In this case, however, the orbital energy is changed resulting in a change in the radius. Both these effects come from a single integration and their quantitative effect as a function of the perturbing frequency is shown in the lower left-hand corner of Fig. IV-1. The energy change produced by an intrack force changes the radius linearly, changing the rate of the displacement intrack linearly. As a result, the intrack displacement increases as a double integration of the intrack perturbing acceleration and therefore is more sensitive to the frequency of the perturbation. The results are shown quantitatively in the right-hand part of Fig. IV-1. One-week perturbations at 10^{-11} g's produce an amplitude

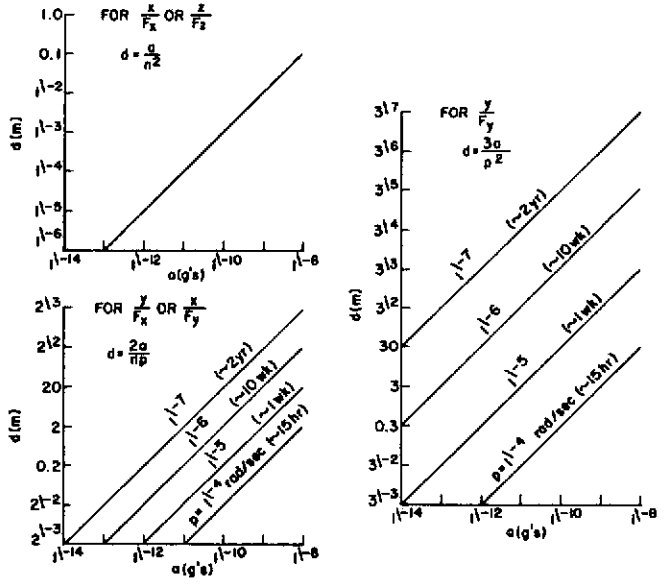

FIG. IV-1. EFFECT OF PROOF MASS DISTURBANCES ON ORBIT

of intrack perturbation that is barely detectable by the most advanced satellite tracking systems.

Disturbances intrack due to an intrack perturbation are the most important perturbations to consider. If the body-fixed disturbing forces that act on the proof mass always were aligned with the orbital axes, it would be possible to put a significantly different specification on the disturbance level for each direction. The normal attitude motions, however, allow what is nominally the vertical or normal axis to have a component along track which would couple as much as 10% of the disturbances in these axes into the intrack direction. For this reason, and because it is very difficult to permit large perturbations in one direction without their appearing in all directions, the specification value for the disturbance level on the proof mass will likely be a single number and used as an isotropic design goal.

For a geodesy mission, intrack perturbations should be minimized since a constant intrack perturbing force of very small magnitude can produce significant changes as long as it acts in the same direction for a long period of time. In Fig. IV-2, the effect of constant intrack perturbations is plotted as a function of time and disturbance acceleration level.

2. Disturbance Force Sources

Though the proof mass is "shielded" from the external environment and thus from the large surface force effects of atmospheric and solar radiation drag, there remain many other smaller sources of force on the proof mass. An exhaustive list of these sources, the relationships governing them, and calculations of representative magnitudes, has been published by Lange [Ref. 2]. The dominant force is the mass attraction of the vehicle for the proof mass. This force will be discussed in more detail in the following sections. In order of size, the next two effects are the electric field forces of the position sensor and the magnetic force due to magnetic field gradients in the cavity. Other forces produce less than 10^{-13}g disturbance.

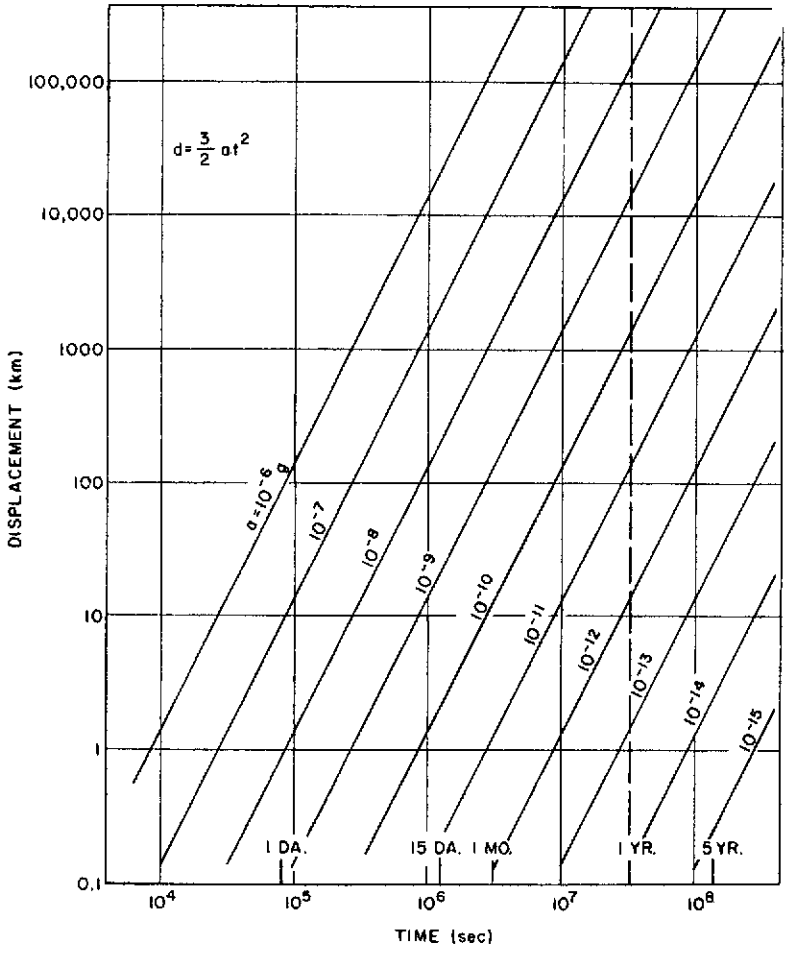

FIG. IV-2. EFFECT OF CONSTANT INTRACK PERTURBATIONS

If an electrostatic position sensor is used, careful design of the position sensor geometry and excitation levels will yield electric field specific forces no larger than 0.2×10^{-11} g. For optical sensors, the forces are even less--on the order of 1×10^{-13} g or less.

The effect of magnetic field gradients can be minimized by minimizing the magnetic susceptance of the proof mass. This can be done by making it of an alloy of a diamagnetic material, such as gold, and a paramagnetic material, such as platinum. It is estimated that with a 70/30 mix of gold and platinum, the magnetic specific forces will be less than 10^{-12} g.

3. Mass Attraction

a. General design considerations. The largest force exerted on the proof mass is due to the mass attraction of the vehicle. Since some relative motion of proof mass beyond the controller deadband is necessary to actuate the controller, and since there will be position sensor null uncertainties, the proof mass will never be exactly at the geometric center of the cavity. Thus, the force due to mass attraction force gradient, as well as the direct force, must be considered as a mass attraction disturbance to the proof mass. The specific force exerted by a particle of mass M at distance R is

$$f = \frac{F}{m} = \frac{GM}{R^2} \frac{R}{|R|}$$

where $G = 0.667 \times 10^{-10}$ N m^2/kg^2. The force due to an extended body is the vector sum of the force of each element of mass. The gradient of this force vector is a dyadic representing the rate of change of force with position of the proof mass.

If the vehicle could be built as a perfect sphere of uniformly distributed mass with a hollow cavity at the center, there would be no vehicle mass attraction for the proof mass anywhere in the cavity. This is not practical, but the vehicle mass distribution should be made as symmetrical as possible and parts should be kept as far as possible from the proof mass. In this way, there is at least some

cancellation of mass attraction forces, and an attenuation due to the $1/R^2$ dependence of the forces.

b. Mass attraction as a function of vehicle geometry. The magnitudes of expected mass attraction specific forces and force gradients at the sensor null point are very much dependent on vehicle geometry. Two different vehicle concepts will be discussed to illustrate the magnitudes of the mass attraction forces.

For an 80 kg gravity stabilized vehicle with 85% of the vehicle mass at the ends of 3 m booms on either side of the vehicle mass center, and 15% contained within a 0.3m × 0.3m cylinder at the mass center, the total uncompensated mass attraction specific force is about 2×10^{-10}g. The specific force gradient components have magnitudes of about 1×10^{-11} g/mm. These are the body-fixed forces. To achieve a total intrack contribution of less than 10^{-11}g, one can very carefully calculate the forces and use small compensation mass to trim (an approach which is extremely tedious and expensive since the calculation accuracy required is about 0.1% for most of the major components). Conversely, the vehicle can be spun about the vertical axis with a vertically oriented momentum wheel in one of the end bodies to cancel vertical momentum. As discussed in Section C, this spinning reduces the intrack effect of the forces in the plane of spin to an acceptable level, but a 1% level of mass distribution bookeeping and compensation is still required to insure that the axial force intrack component due to attitude libration is less than 10^{-11}g.

The second concept is a spin-stabilized vehicle orientated with its spin axis nominally normal to the orbit plane. In this case, the total vehicle mass is much closer to the proof mass so the general mass attraction force environment is stronger. The mass attraction forces in the plane normal to the spin are attenuated due to spin averaging so the dominant intrack perturbations are due to the intrack component of axial force from attitude errors, and proof mass intrack hang-off with respect to the sensor null in the presence of mass

attraction gradient (Section C). To achieve the total body-fixed mass attraction specific force of 3×10^{-10}g and force gradient of 3×10^{-10}g/mm used as a basis for the preliminary vehicle configuration in Section E, it is required that the vehicle mass distribution be calculated and compensated to about 1 percent.

B. TRAPPING CONSIDERATIONS IN THE DESIGN OF SPINNING SATELLITES

The design of a translation controller for a spinning satellite typically includes a deadspace to eliminate chatter. This design feature and the inability to locate precisely the center of mass give rise to a phenomenon called trapping that potentially could waste significant amounts of propellant during periods of no external disturbing forces. A theory has been developed and experimentally verified that explains the role of these factors and provides insight into the effect of other control parameters. A detailed description of the analysis and experimental verification of the trapping phenomenon is contained in Ref. 15. The following is a summary of this material.

The trapping phenomenon is simply a stable equilibrium of the vehicle/controller equations of motion that continuously uses propellant. Such equilibrium points are expected in the presence of large disturbing forces or large center-of-mass (c.m.) offsets; however, the more important aspect is that the phenomenon is possible with no disturbing forces and no c.m. offsets. Careful selection of the deadspace shape and control system parameters minimizes the susceptibility of a system to becoming trapped; however, in many missions, use of a c.m. estimator will be required to eliminate the c.m. location uncertainty as a source of trapping and its associated propellant wastage.

A linear translation control law for a spinning satellite [Ref. 16] in the plane of spin is

$$f_{cx} = -k_p\left[x_b + \gamma(u_b - \omega_s y_b)\right]$$
$$f_{cy} = -k_p\left[y_b + \gamma(v_b + \omega_s x_b)\right] \qquad (4.1)$$

where

f_{cx}, f_{cy} = the control forces

k_p = the position gain

γ = the ratio of velocity to position gain

ω_s = the satellite spin rate

x_b, y_b = the proof mass position coordinates relative to the satellite

u_b, v_b = the proof mass velocity coordinates relative to the spinning satellite.

The spin dynamics do not affect the control along the spin axis; therefore, in studying the effects of spin, this direction need not be considered.

This linear control law has been modified by some form of a deadspace in the laboratory mechanizations at Stanford. One natural mechanization is the square deadspace which is defined in Fig. IV-3

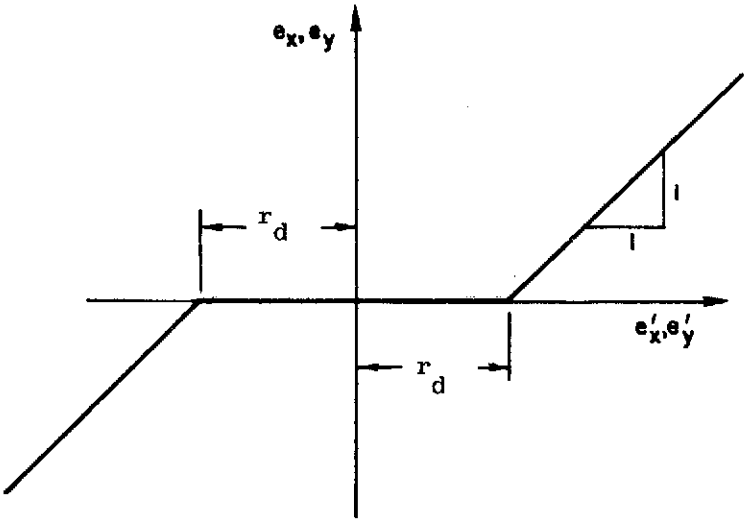

FIG. IV-3. SQUARE DEADSPACE DEFINITION

where

$$\begin{aligned} e'_x &= x_b + \gamma(u_b - \omega_s y_b) \\ e'_y &= y_b + \gamma(v_b + \omega_s x_b) \end{aligned} \tag{4.2}$$

$$\begin{aligned} f_{cx} &= -k_p e_x \\ f_{cy} &= -k_p e_y \end{aligned} \tag{4.3}$$

Another mechanization results in a circular deadspace and is given by

$$\left.\begin{aligned} e_x &= e'_x - \frac{e'_x}{r} r_d \\ e_y &= e'_y - \frac{e'_y}{r} r_d \end{aligned}\right\} \text{if} \quad r > r_d$$

$$\left.\begin{aligned} e_x &= 0 \\ e_y &= 0 \end{aligned}\right\} \text{if} \quad r \leqslant r_d \tag{4.4}$$

where

$$r = \sqrt{e'^2_y + e'^2_x}\,.$$

r_d = size of deadspace in both x and y directions .

The factors influencing the trapping phenomenon are:

(1) the location of the center of mass,

(2) the deadspace shape and size, r_d

(3) control parameters: k_p, ω_s, γ .

Typically, the nondimensional parameter k_p/ω_s^2 will be $\gg 1$. This is necessary for well-damped controller roots as well as satisfying a requirement that the controller be able to provide sufficient thrust to capture the proof mass when initially riding on the cavity walls.

Assuming $k_p/\omega_s^2 \gg 1$, Fig. IV-4 shows the amount of c.m. offset allowable before trapping occurs. The importance of deadspace shape and the control parameter $\gamma\omega_s$ is demonstrated in the figure. Note that for a square deadspace, the controller will be trapped with no c.m. offset if $|\gamma\omega| < 1$. For $k_p/\omega_s^2 < 1$, the system is much less susceptible to trapping. See Ref. 17 for a detailed analysis of this class of systems.

Most practical control mechanizations will include on-off propulsive devices. Therefore, even during periods of zero disturbing forces, a limit cycle will exist which uses propellant. For an assesssment of the importance of the trapping phenomenon, its control effort (or propellant consumption) must be compared with a system which is not trapped (or "limit cycling"). Typical on-off controllers for $1/s^2$ plants limit cycle with a phase plane trajectory as shown in Fig. IV-5 when there are no disturbing forces [18]. The control effort during these limit cycles is

$$w = \frac{1}{4}\frac{(\Delta v)^2}{d_s} \tag{4.5}$$

where

$\Delta v \triangleq$ minimum permissible impulse

$d_s \triangleq$ deadspace size .

In a two-axis non-spinning system, both axes are simultaneously in the limit cycle, therefore

$$\dot{w} = \frac{1}{2}\frac{(\Delta v)^2}{r_d} \quad . \tag{4.6}$$

In a spinning $1/s^2$ system, no stable limit cycles have been observed, but experimental observations of control effort on the laboratory simulator approximate that given by Eq. 4.6. Therefore, a spinning system with no external disturbing forces acting on it is either in a limit cycle requiring the control effort given by Eq. 4.6, or it is trapped requiring a control effort given by the trapped equilibrium solution.

$$r^* = \frac{\text{center-of-mass offset allowable}}{\text{deadspace radius}}$$

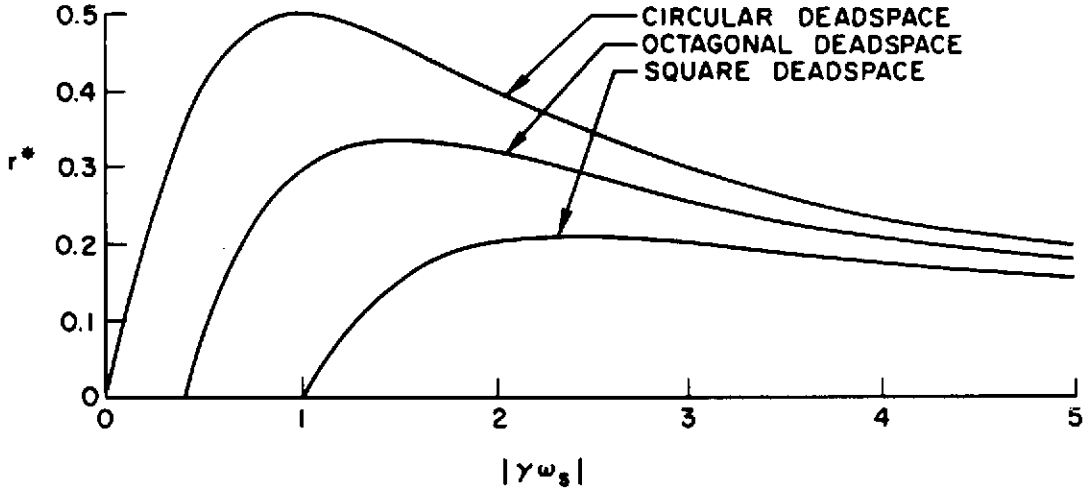

FIG. IV-4. r^* FOR CIRCLE, SQUARE, AND OCTAGON

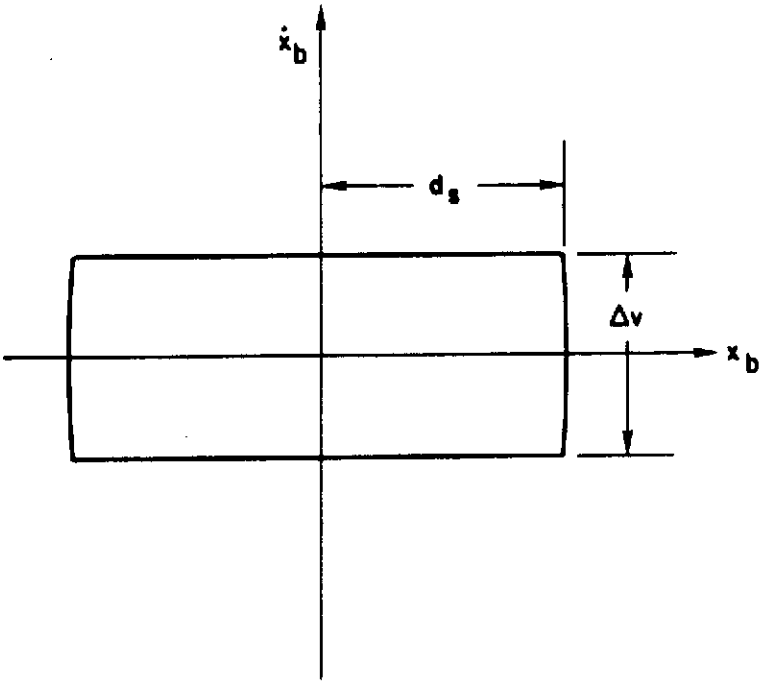

FIG. IV-5. TYPICAL ONE-AXIS LIMIT CYCLE WITH NO DISTURBING FORCES.

Figures IV-6 and IV-7 show the control effort vs c.m. for several selected values of control parameters, as well as the square and circular deadspaces. The nondimensional parameter $(k_p/\omega_s^2) = 15$ in both figures which represents the class of controllers where $k_p/\omega_s^2 \gg 1$. In Fig. IV-6 the control effort takes a jump upward from the limit cycling value given by Eq. 4.6 to the $\dot{w}$ resulting from the trapped equilibrium solution for the square and circular deadspace. The jump occurs at the c.m. displacement equal to r^* (see Fig. IV-4) for the corresponding deadspace shape. Two of the curves drawn in Fig. IV-6 represent the $\gamma\omega_s$ yielding the maximum r^*, one curve represents the mechanized values on the laboratory simulator ($\gamma\omega_s = 1$, square deadspace) before knowledge existed of the trapping phenomenon, and the lower curve represents a control law with the estimated c.m. location as the control center, thereby eliminating $\dot{w}$ dependence on the c.m. location. The fact that the trapped control effort in Fig. IV-6 is higher in all cases than the limit cycling control effort is a result of the value chosen for the nondimensional minimum impulse parameter $\Delta v/r_d\omega_s$. In Fig. IV-6, $\Delta v/r_d\omega_s$ was chosen to be $2/3$, a value representing the maximum jet pressure on the laboratory simulator at $\omega_s = 1$ rad/sec. Most drag-free satellite designs considered have typical values of $\Delta v/r_d\omega_s < 2/3$ at $\omega_s \geq 0.1$ rad/sec and the conclusions from Fig. IV-6 are not changed for these cases. For the class of systems represented by Fig. IV-6, the penalty in control effort due to the trapping phenomenon is substantital and systems should be designed to minimize the possibility of this event.

Given any minimum impulse (Δv) and deadspace (r_d), it is always possible to pick the spin rate (ω_s) low enough so that $\Delta v/r_d\omega_s \gtrsim 4/3$. This case is represented in Fig. IV-7 and for this class of systems, the trapping phenomenon is not as important a design factor. Since the control effort due to the phenomenon is that required to maintain the c.m. in a circular trajectory at the spin rate, the result that lowering the spin rate decreases the importance of the phenomenon is not unexpected.

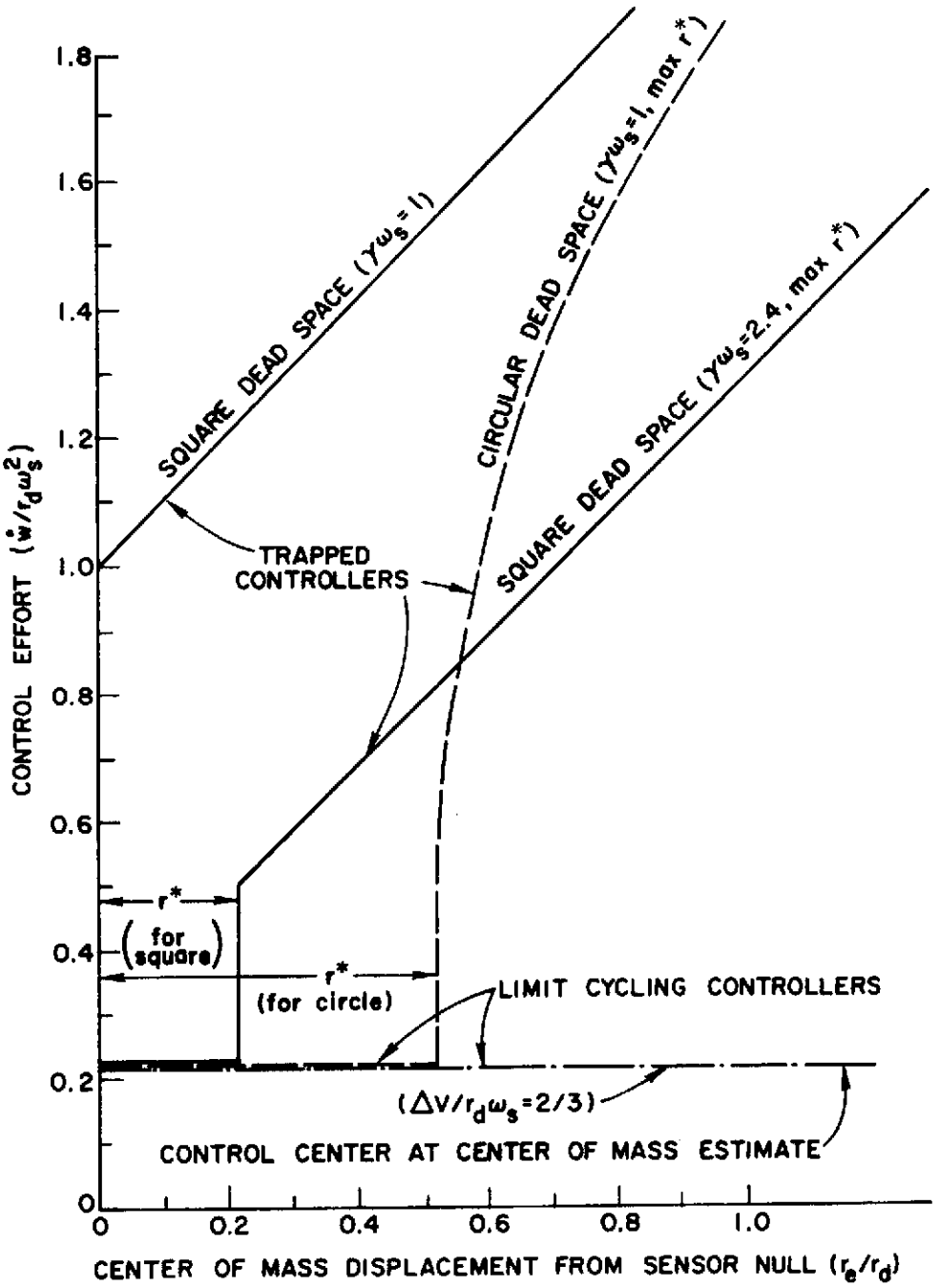

FIG. IV-6. CONTROL EFFORT VS CENTER OF MASS ($\Delta v/r_d\omega_s = 2/3$).

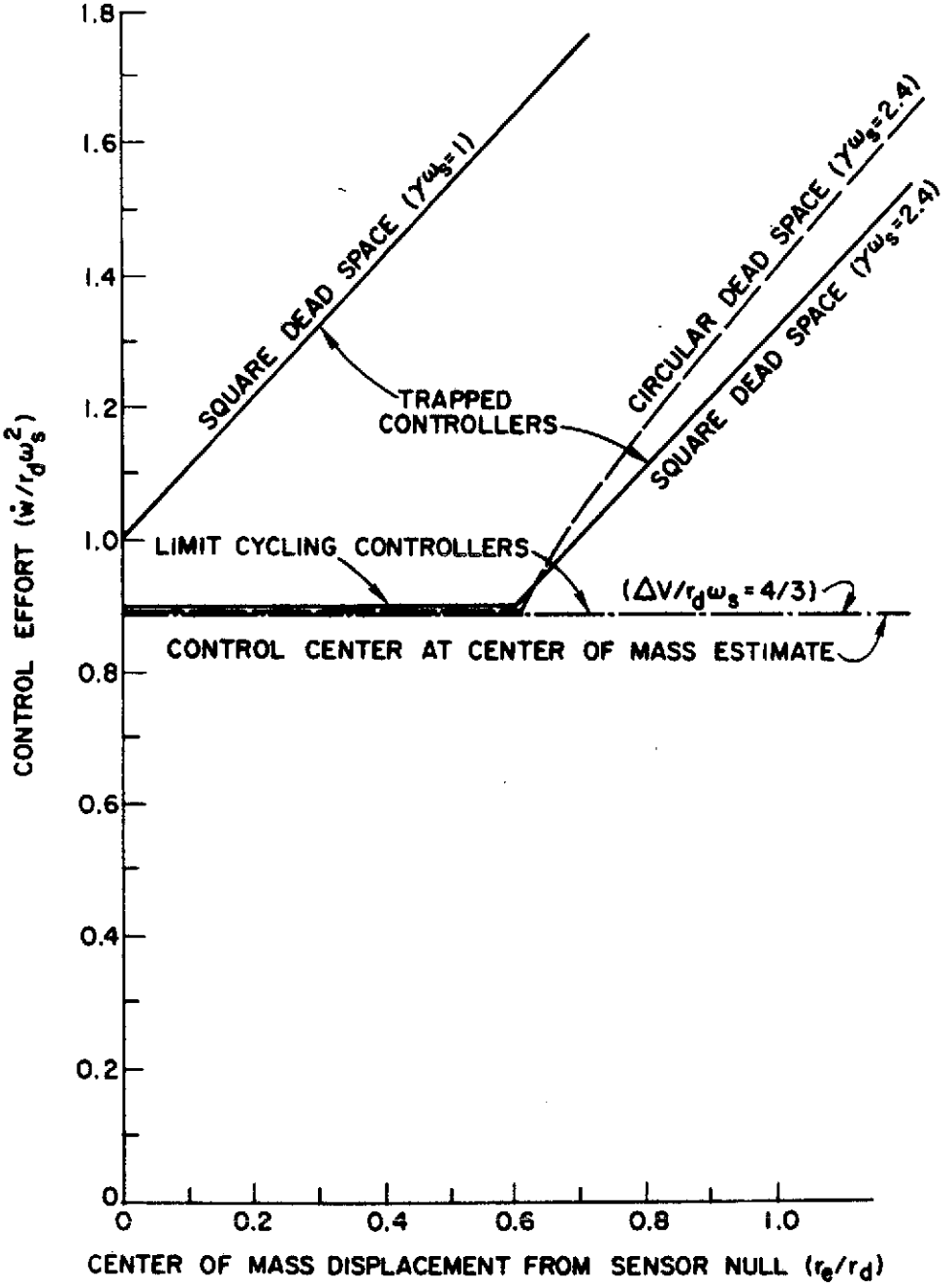

FIG. IV-7. CONTROL EFFORT VS CENTER OF MASS ($\Delta v/r_d\omega_s = 4/3$).

The analysis of the trapping phenomenon has assumed the existence of the ω_s cross-coupling terms in the control law. For very low spin rates, it may be desirable to omit these terms. The analysis of the phenomenon applies to this case if $\gamma\omega_s$ is assumed equal to zero. Figure IV-4 indicates that the system is trapped for all deadspace shapes with no c.m. offset when $\gamma\omega_s = 0$. As a result, to avoid propellant wastage in spinning drag-free satellites without the $\gamma\omega_s$ cross-coupling terms, $\Delta v/r_d\omega_s$ must be $\gg 1$.

The validity of the trapping phenomenon analysis has been verified experimentally on a laboratory simulator of the drag-free satellite translation control system. The simulator floats on an air bearing over a level granite table [Ref. 19] about a proof mass which is attached to the table. Thus, the orbital equations of motion of the relative position between satellite and proof mass are duplicated in the laboratory. External disturbing forces are simulated by introducing a bias in the table leveling device, thus producing accurate, small (< 1 arc sec) table tilt angles. A small analog computer adjacent to the simulator aided in the data evaluation. Figure IV-8 is a picture of the laboratory apparatus.

Associated with the trapping verification is the c.m. estimation research. The analytical aspects of these concepts have been reported previously in Ref. 8, and a detailed description is contained in Ref. 15. By estimating the c.m. and controlling to this location rather than the position sensor null point, c.m. offsets are eliminated as a factor in the trapping phenomenon and the design requirements of a spinning drag-free satellite are simplified. Figure IV-9 is a picture of the electronic package with one of the two c.m. estimator cards extended for viewing.

The control law in the simulator was mechanized with a circular deadspace and the c.m. estimator on an optional basis. Without the c.m. estimator operative, the control effort was determined at various locations of the c.m., thus experimentally duplicating the analytical curves given in Fig. IV-6. This comparison is shown in Fig. IV-10.

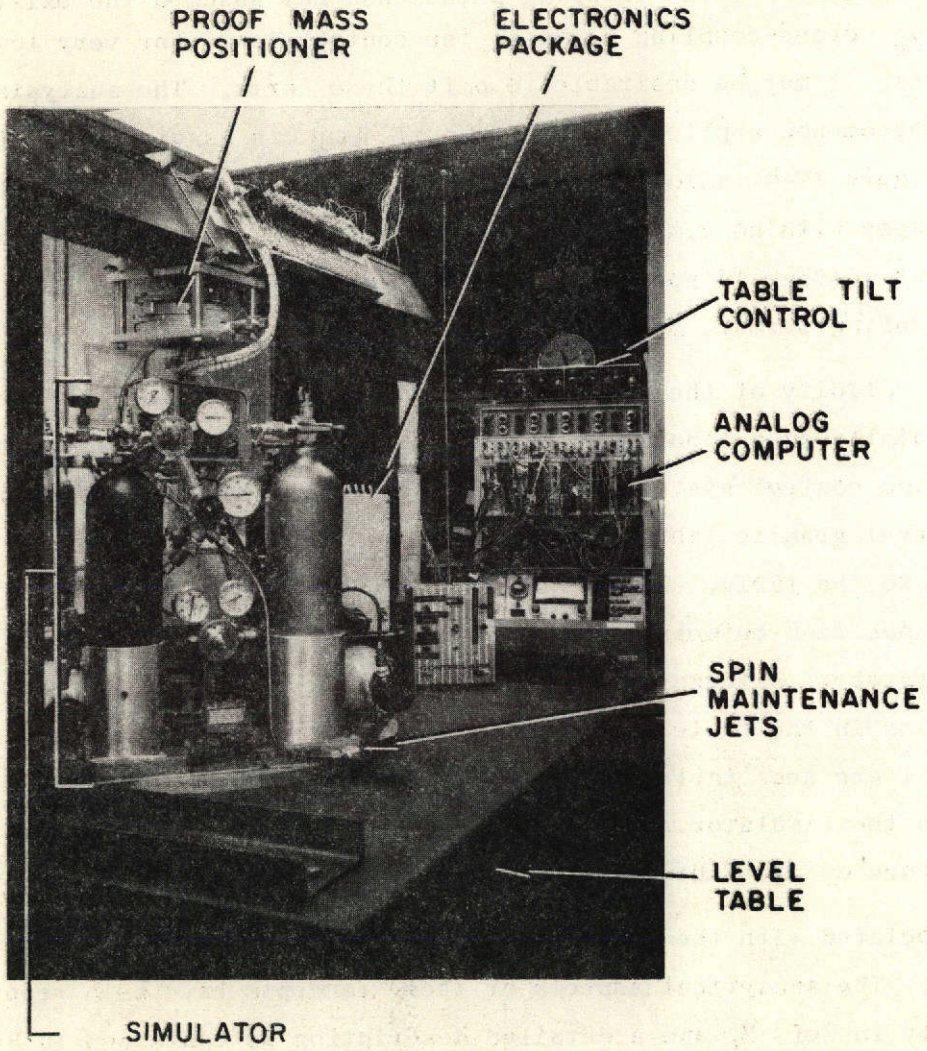

FIG. IV-8. EXPERIMENTAL APPARATUS

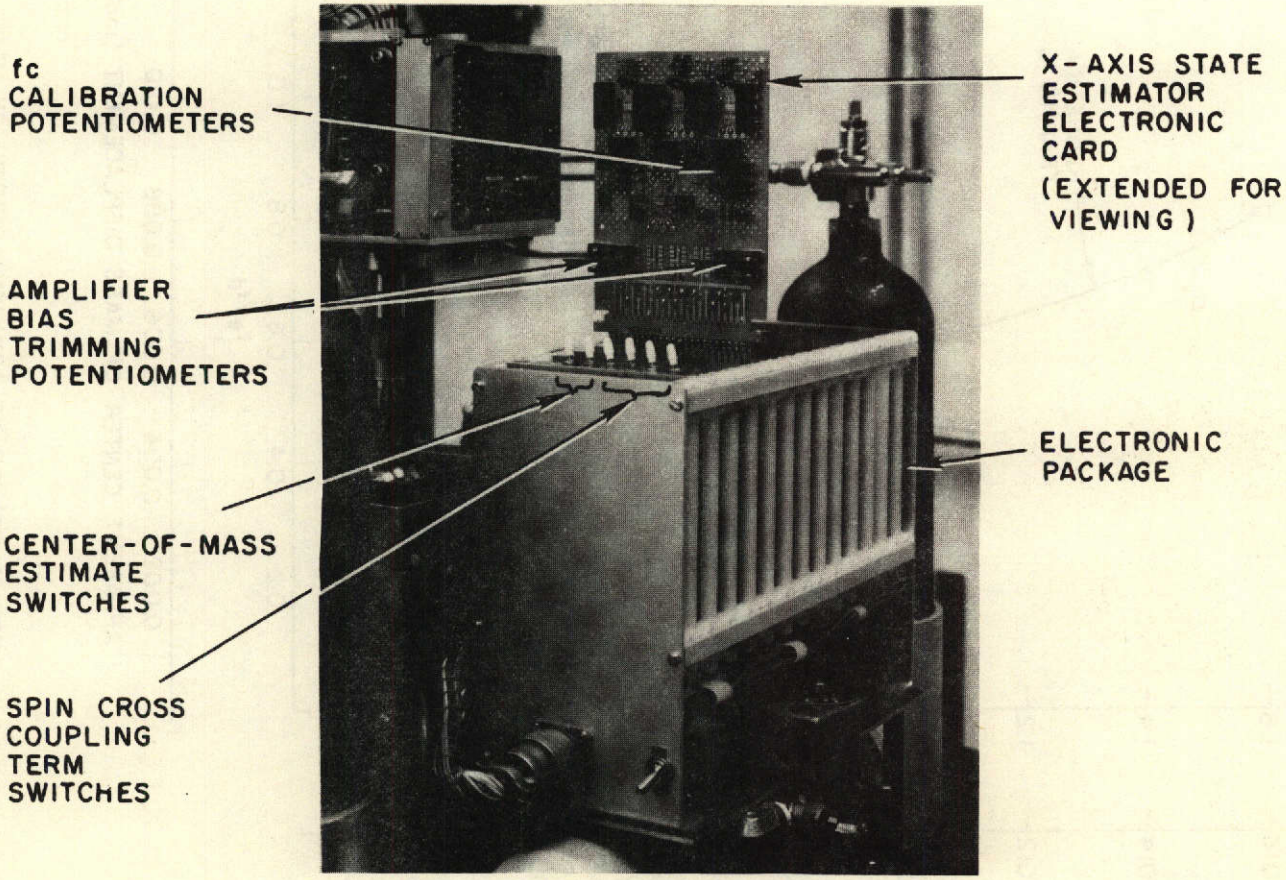

FIG. IV-9. SIMULATOR ELECTRONICS

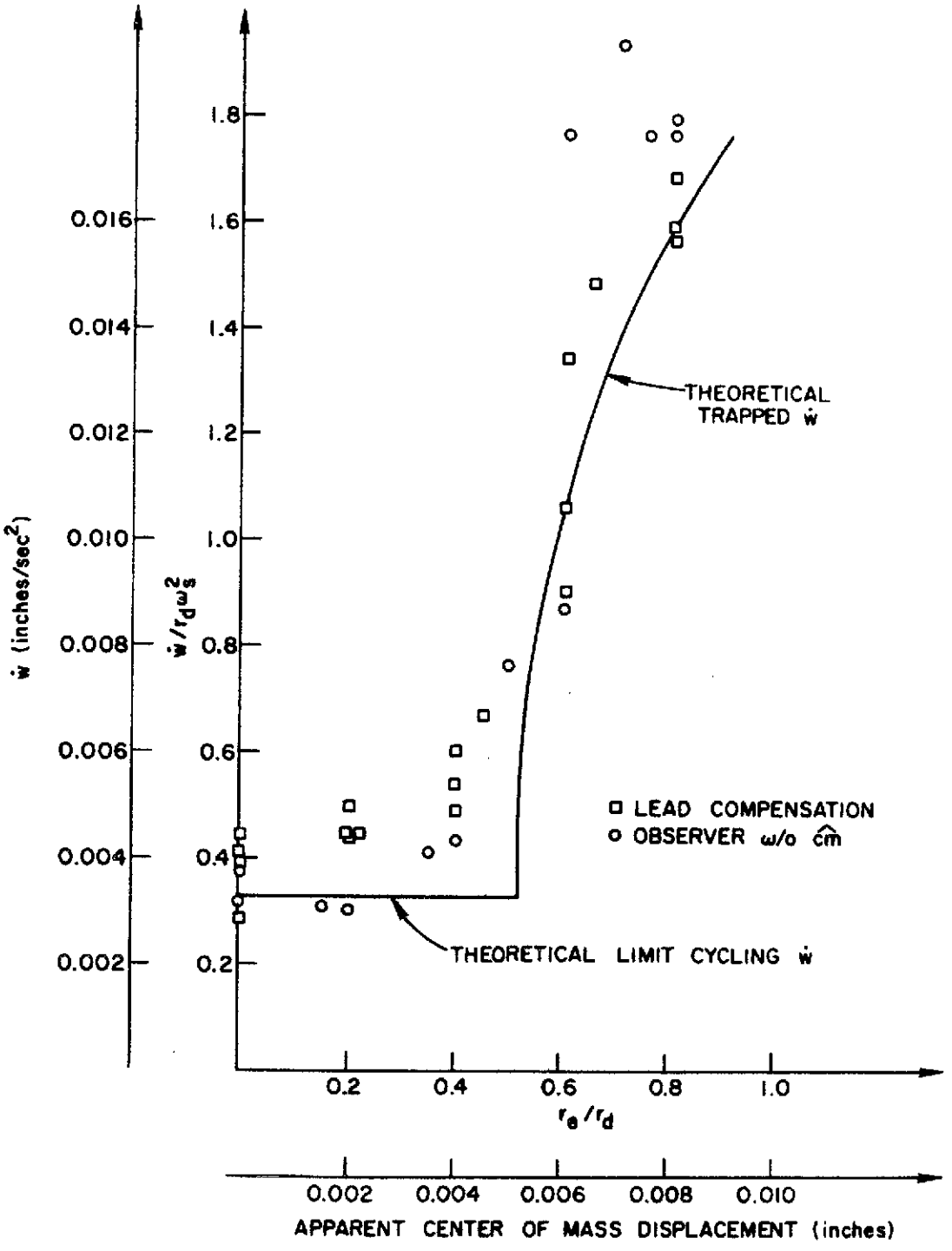

FIG. IV-10. CONTROL EFFORT VS APPARENT CENTER OF MASS

The control effort was also determined with the c.m. estimator operative and, as expected, the c.m. location had very little influence on it. These results are shown in Fig. IV-11.

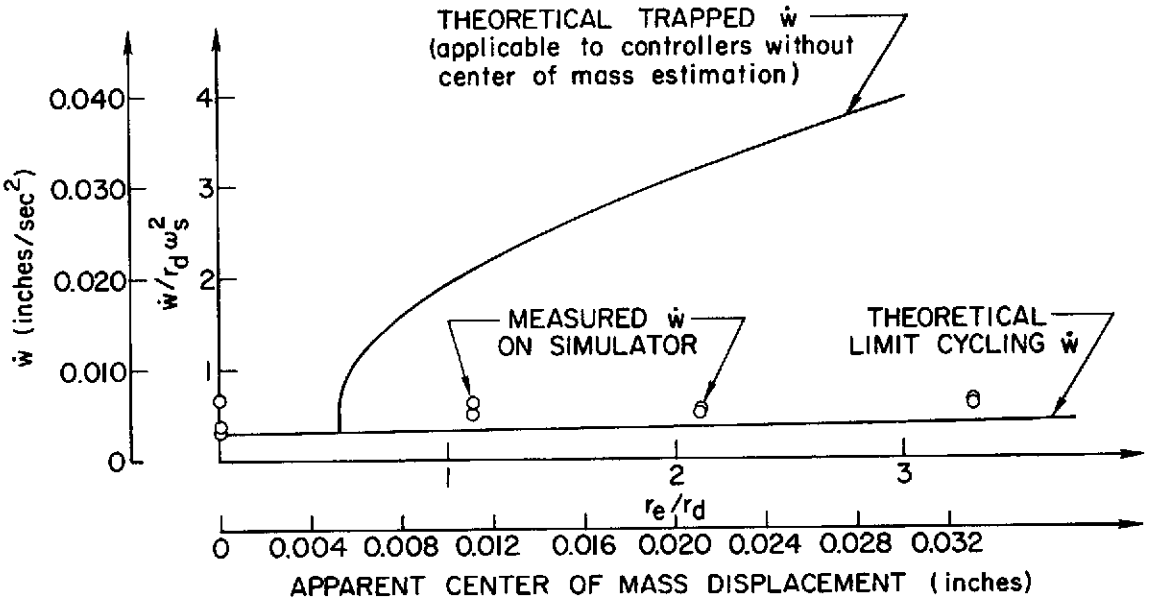

FIG. IV-11. CONTROL EFFORT VS CENTER OF MASS WITH CENTER-OF-MASS ESTIMATION

In summary, the trapping phenomenon has been analyzed in detail with the important aspects verified experimentally. The important parameters are $\gamma\omega_s$, the deadspace shape, c.m. location uncertainty, and $\Delta v/r_d\omega_s$. If $\Delta v/r_d\omega_s \ll 1$, trapping is an important design consideration, and the deadspace shape and $\gamma\omega_s$ must be selected carefully to minimize the effects of the phenomenon. The expected error in physically locating the center of mass and the sensor null at the same point and maintaining the alignment throughout the satellite lifetime determines whether c.m. estimation techniques also must be employed in these cases. If $\Delta v/r_d\omega_s \cong 1$, trapping is not a major design factor; however, control effort can be reduced by judicious selection of $\gamma\omega_s$. If $\Delta v/r_d\omega_s \gg 1$ (typically only true when $\omega_s \ll 0.1$ rad/sec), trapping considerations can be ignored.

This analysis has shown the conditions that must be met to prevent possible propellant wastage caused by the trapping phenomenon. The experimental results reveal that, when not trapped and when no external forces are present, the propellant consumption in the spinning case approximates the theoretical nonspinning propellant consumption. As a result, if a spinning drag-free satellite is designed so that the trapping phenomenon will not occur, no penalty in propellant for translation control is incurred by the spin.

C. INTEGRAL CONTROL OF A SPINNING DRAG-FREE SATELLITE TO REDUCE TRAJECTORY ERRORS DUE TO MASS ATTRACTION

The mass attraction force of the satellite on the proof mass is the largest force perturbing the satellite from an orbit which is solely under the influence of planetary gravity. For some drag-free satellite applications, it is desirable to reduce the effect of this perturbation force.

1. Disturbing Forces on the Satellite

Since the satellite will be spinning, the mass attraction force at the sensor null point will not produce long-term trajectory errors. However, due to the inability to precisely locate every mass element in the satellite, there will be non-zero mass attraction gradients. This implies that forces which disturb the satellite may result in a mass attraction force on the proof mass due to the gradients.

A disturbing force which is fixed to the satellite (e.g., control jet gas leak) will cause a proof mass displacement which is constant in any satellite fixed reference frame. Therefore, any resulting mass attraction force will be modulated by the satellite spin, and no long-term trajectory error will result.

Of the disturbance forces not fixed to the satellite, only the constant atmospheric drag force will cause significant trajectory errors. The reason is that in the presence of constant atmospheric drag, the proof mass displacement, and the resulting force caused by

mass attraction gradients, will be systematically in the intrack direction. Hence, the mass attraction force is not averaged by the satellite spin and will cause an intrack trajectory error on the order of 150 km after one year*.

2. Integral Control Equations

To reduce trajectory errors caused by mass attraction force, a control center bias

$$\begin{bmatrix} x_u \\ y_u \end{bmatrix} = -k_c \begin{bmatrix} c & -\Delta \\ \Delta & c \end{bmatrix}^{-1} \begin{bmatrix} I_{hc} \\ I_{vc} \end{bmatrix} \tag{4.7}$$

where

$k_c \triangleq$ integral control gain

$c \triangleq \cos(\omega_{ht})$

$\Delta \triangleq \sin(\omega_{ht})$

$\omega_h \triangleq$ satellite spin frequency plus orbital frequency

$$\begin{bmatrix} I_{hc} \\ I_{vc} \end{bmatrix} \doteq \int_o^t \begin{bmatrix} x_{bi} \\ y_{bi} \end{bmatrix} dt \tag{4.8}$$

$$\begin{bmatrix} x_{bi} \\ y_{bi} \end{bmatrix} = \begin{bmatrix} c & -\Delta \\ \Delta & c \end{bmatrix} \begin{bmatrix} x_b \\ y_b \end{bmatrix} \tag{4.9}$$

---

* This was calculated in Ref. 15 assuming a first-order mass attraction gradient of 10^{-10} g/mm and

$$\frac{\text{drag force}}{(\text{satellite mass})(\text{control gain})} = 0.1 \text{ mm} .$$

is introduced. The control law then becomes

$$f_{cx} = -k_p[x_b - x_u + \gamma(u_b - \omega_s y_b)] \tag{4.10a}$$

$$f_{cy} = -k_p[y_b - y_u + \gamma(v_b + \omega_s x_b)] \tag{4.10b}$$

where f_{cx}, f_{cy}, k_p, x_b, y_b, u_b, v_b, γ, and ω_s are as defined in Section B.

The bias acts to move and keep the proof mass at the control sensor null point in the presence of constant atmospheric drag.

3. Stability Analysis of Integral Control

Through the use of frequency symmetry [Ref. 17], a root locus can be constructed for the integral controlled system. This is done in Fig. IV-12 for two values of k_p. Note that only half of the root locus plot is shown; and that the complete plot is symmetric about the σ axis. Three parameters are needed to define the root locus locations, $\gamma\omega_s$, k_p and k_c. k_p is lower bounded by the fact that it must be large enough to move the proof mass away from the cavity wall if it were pushed against the wall at spinoff from the booster. This requires

$$-f_c = k_p r_c > \omega_s^2 r_c$$

or

$$k_p > \omega_s^2 \tag{4.11}$$

where $r_c \triangleq$ radius of the satellite cavity.

Increasing $\gamma\omega_s$ moves the pole at -0.1, 0.1 in Fig. IV-13 towards the $j\omega$ axis, while decreasing $\gamma\omega_s$ moves it away from the $j\omega$ axis. Therefore, $\gamma\omega_s$ must be low enough ($\lesssim 3$) such that there is sufficient damping. A third consideration in choosing $\gamma\omega_s$ is trapping susceptibility discussed in Section B.

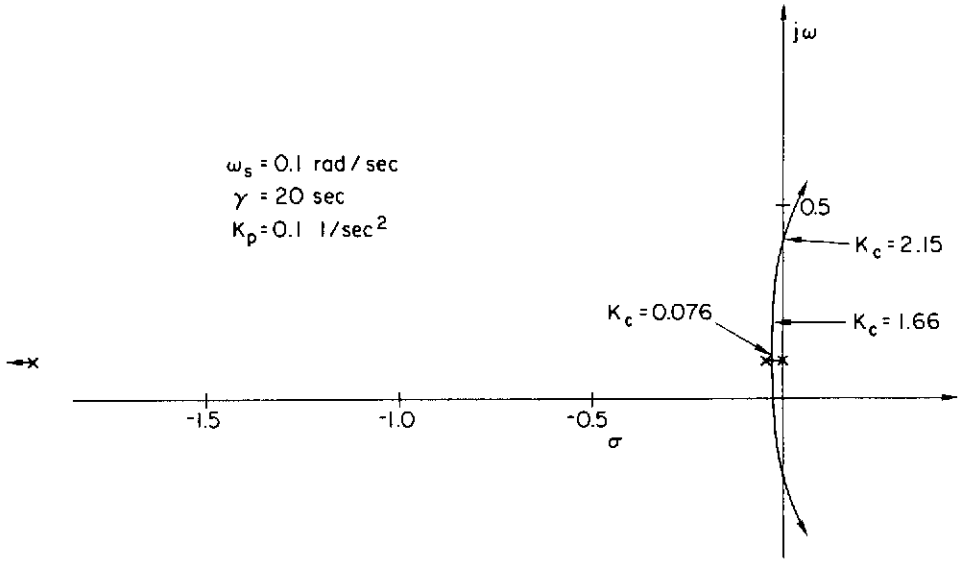

FIG. IV-12. ROOT LOCUS PLOT VS K_c

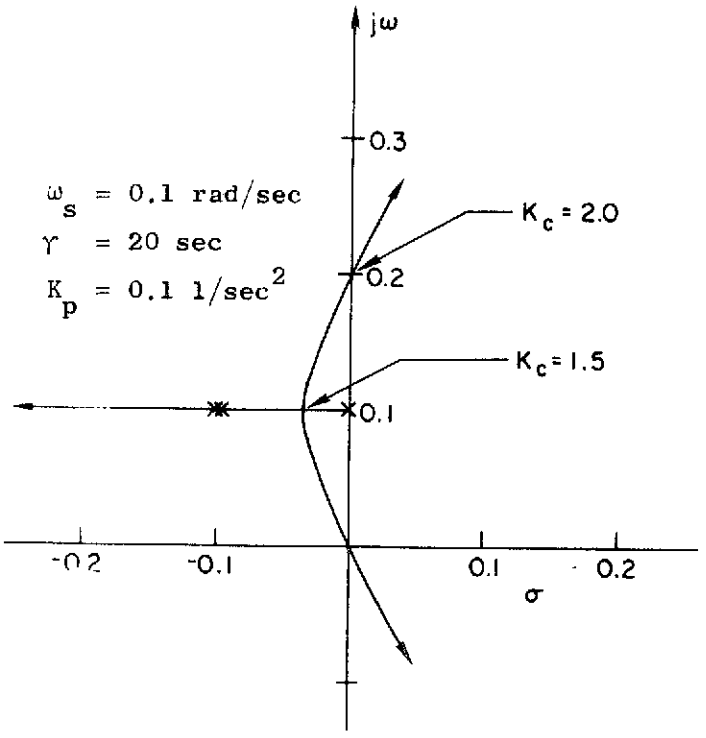

FIG. IV-13. ROOT LOCUS PLOT VS K_c

4. Effectiveness of Integral Control

Computer simulations of integral on-off control with deadspace [Ref. 17], which will be used in practice, showed that the stability analysis of the preceding section is valid. Figure IV-14 shows a plot of $x_{bi}(t)$ obtained from these simulations.

These simulations showed that $k_c \ll \omega_s$ is necessary to avoid interference with the basic non-integral translational control, in agreement with the root locus analysis.

With on-off control, the proof mass is not driven and kept at the sensor null point. This is expected, since the control force magnitude cannot be decreased, as needed when the proof mass is very close to the null point, and overshoot occurs. This implies a nonzero average mass attraction force. Assuming the same values as in Section 1 above, the trajectory error of 150 km is reduced to 72 m with the use of a perfectly mechanized integral, on-off control with deadspace.

In mechanizing an on-off integral controller with deadspace, there are several factors which may cause a total intrack trajectory error (due to mass attraction) of more than 72m per year. These are analyzed below.

5. Mechanization Errors

The error analyses were done with the following assumptions:

(1) mass attraction gradient in the orbital plane is equal to 10^{-10}g/mm, and the mass attraction force normal to the orbital plane is equal to $3\ 10^{-10}$g;

(2) no knowledge of the mass attraction properties of the satellite is assumed;

(3) control gain $k_c = 4 \times 10^{-3}$ 1/sec.

(4) digital mechanization of the controller equations;

(5) spin rate $\omega_h = 0.1$ rad/sec;

(6) atmospheric drag acceleration of 10^{-3} to 10^{-5} mm/sec^2.

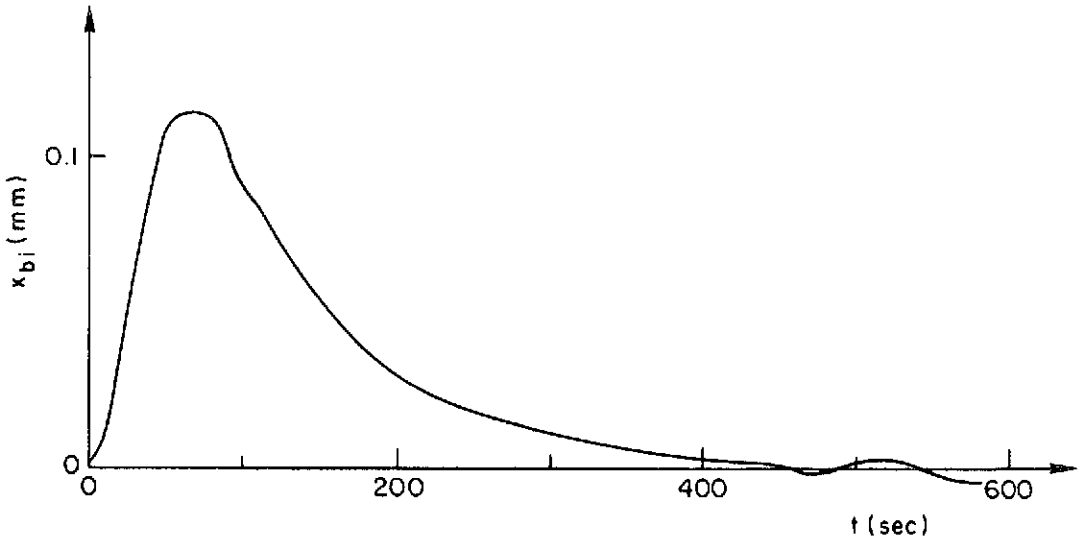

FIG. IV-14: PLOT OF $x_{bi}(t)$ FROM COMPUTER SIMULATION OF THE INTEGRAL CONTROLLED SYSTEM (on-off with deadspace) WITH

k_c = 0.004 1/sec

deadspace size = 0.1 mm

control force level = 0.05 mm/sec^2

control pulse width = 0.02 sec

a. Spin rate mechanization error. With a spin rate (ω_h) mechanization error of 10^{-3} rad/sec, both analytical and computer simulation methods show an intrack trajectory error of approximately 800 m per year. This assumes no horizon information is available to the controller. Because of the magnitude of this error, it may be desirable to update the controller's attitude reference from horizon sensor information.

b. Attitude errors. Assuming a satellite spin axis misalignment with the orbit plane normal of 2 arc sec, a trajectory error of 45 m results.

c. Trajectory error due to limit cycle behavior of the proof mass. With on-off integral control with deadspace, typical time histories of the proof mass position are limit cycles about the sensor null point. If this limit cycle's frequency $\omega_{\ell c}$, is in resonance with certain multiples of the spin rate, mass attraction gradients will cause long term trajectory errors.

The largest of these trajectory errors, about 100 cm after four months of resonance, occurs if $\omega_{\ell c} = 2\,\omega_h = 0.2$ rad/sec. This error decreases to 2 m if $\omega_{\ell c} = 2\,\omega_h + 10^{-5}$. Since $\omega_{\ell c}$ is proportional to the atmospheric drag force, the orbital altitude can be chosen such that $|\omega_c - 2\,\omega_h| < 10^{-5}$ rad/sec. The other resonant frequencies ($\omega_{\ell c} = \omega_h$, $\omega_{\ell c} = 2/3\,\omega_h$, etc.) cause maximum trajectory errors of much less than 100 m.

6. Conclusion

This controller can reduce intrack trajectory error to 920 m per year (corresponding to an average force of $\sim 10^{-13}$ g). This assumes a spin rate mechanization error of 0.001 rad/sec, a satellite spin axis misalignment with the orbit plane normal of 2 arc sec, and orbital altitude chosen such that the resulting proof mass limit cycle frequency is 10^{-5} rad/sec away from resonant frequencies. Alternately, if the goal of drag-free performance is on the order of 10^{-11} g, the

integral controller has the effect of relaxing the cost and effort required to minimize mass attraction levels in the design and fabrication of the satellite.

D. ATTITUDE/TRANSLATIONAL COUPLING IN A GRAVITY STABILIZED DRAG-FREE SATELLITE

At various points in our work on the application of the drag-free principle to geodesy, it has been suggested that a gravity stabilized vehicle might be used.

For a drag-free, gravity stabilized satellite, the relative position sensor null point and the thrustor lines of action will not be coincident with the vehicle mass center. Thus, attitude motion is sensed by the translational control system and translation control produces moments. The resulting coupling between the attitude and translational motions can cause attitude instabilities. In some cases, the phase shift which degrades the stability is introduced by the orbital dynamics in a unique interaction of the feedback with the passive attitude control and orbital mechanics.

An investigation of the coupling in the plane of the orbit was performed [Refs. 8, 20]. An extension of this work to the roll/yaw motion was performed under Navy sponsorship and the results of this extension are documented in Ref. 21.

In both the planar and roll/yaw cases, the derived relationships are functions of the position sensor null offset, thrustor moment arms and null offsets are less than a few centimeters.

E. PRELIMINARY VEHICLE CONFIGURATION

The guidelines given to Stanford by NASA* for a first geodesy

* Mr. Jerome Rosenberg, NASA Headquarters

drag-free satellite suggested a minimum design containing just those features essential to the drag-free geodesy mission. In keeping to these guidelines, the philosophy has been to select the simplest satellite design which yields adequate drag-free performance to demonstrate the principle and obtain some new geodesy information.

1. Proof Mass Disturbance Considerations

Typical conventional satellites encounter nongravitational specific forces on the order of 10^{-8}g to 10^{-6}g, primarily due to atmospheric drag and solar pressure. In a drag-free satellite, these forces are completely shielded from the proof mass and therefore do not disturb its trajectory. However, other forces do act on the proof mass and must be considered in drag-free satellite design. The major disturbing forces are (refer to IV, Sect. A above)

(a) mass attraction of the outer satellite;

(b) electrostatic force from the capacitive position sensor;

(c) magnetic force from the earth's field.

The last two forces can be limited by careful design to be on the order of 10^{-12}g but are not major design constraints. The mass attraction force of the satellite for the proof mass, is the major disturbing force perturbing the proof mass from an orbit solely under the influence of planetary gravity.

The intrack orbit direction is significantly more sensitive (see IV, Sect. A above) to disturbing forces than the other axes. Therefore, the constant body-fixed portion of the mass attraction forces can be averaged in this sensitive axis by spinning the satellite about an axis normal to the intrack direction. Typically, the mass attraction forces are predominately constant body-fixed; therefore, spinning provides a substantial reduction in orbit perturbations due to mass attraction forces. This factor and simplified attitude control provide the motivation for spinning the satellite.

2. Tracking Considerations

In Section I, two distinct drag-free missions were discussed. For determining spatial variations in the gravity field, a low orbit is desirable and satellite-to-satellite tracking and very high tracking accuracy (1 meter) are essential. For determining temporal variations in the gravity field, a 1050 km circular orbit is recommended and satellite-to-satellite tracking is recommended but not essential. Tracking accuracy need not be great since very long term effects are of interest. To track a drag-free satellite from synchronous orbit requires a highly directional antenna (approximately 10 db gain in the synchronous satellite direction and introduces a complication in the design of any satellite but particularly in a spinning satellite. Antenna directionality in spinning satellites has been achieved by despinning the antenna either electrically or mechanically. Because of the desirability of rotating all satellite parts about the proof mass to average the mass attraction forces, an electrically despun antenna is the preferred choice if satellite-to-satellite tracking is used.

3. Satellite Configuration

The simplest satellite consistent with the NASA Guideline, and able to fly at the earliest date (even before satellite-to-satellite tracking is a reality) will

(1) be spin stabilized to obtain a high degree of cancellation of internal proof mass perturbation without excessive costs;

(2) emphasize the determination of the temporal gravity variation (i.e., 1050 km circular orbit) although some higher harmonic data will be obtained;

(3) not use satellite to satellite tracking on the first flight.

The decision to spin is primarily influenced by the reduced effort and cost required in the design and construction of the satellite to achieve low mass attraction force levels. Satellites designed for determination of the temporal gravity variations yield a simpler

design because characteristics of the long term drift over many orbits are sought in this mission and therefore high precision tracking is not essential. Satellite-to-satellite tracking, while offering great potential for precision tracking if available for the first mission and especially for subsequent low altitude missions, is not an essential element of the high altitude mission.

In the event that satellite-to-satellite tracking is available, the choice of a spinning satellite is not so clear. The mass attraction design complications in a nonspinning spacecraft must be weighed against the antenna despin complications in light of the mission requirements which involves both the level of perturbations and tracking to decide if the spinning satellite remains the attractive design.

4. Spin Orientation

In the discussion of the relationship between spin and mass attraction effects, it was stated that the spin axis must be perpendicular to the orbit intrack direction. Spin axes aligned either normal to the orbit plane or with the vertical are therefore possible choices. Spin about the vertical requires a momentum cancelling wheel to allow earth rate precession and makes gravity gradient attitude stabilization possible. Spin about the orbit normal requires an active attitude control system, however, the spin itself provides a stable reference. Attitude control accuracy is also a factor since misalignments of the spin axis cause mass attraction forces along the spin axis to couple into the sensitive intrack direction. The best compromise between simplicity and attitude control accuracy was judged to be the configuration with active attitude control and spin about the orbit normal.

5. Design Features

A preliminary drag-free satellite design based on the fundamental considerations described above is depicted in Fig. IV-15. The design is based on a cold gas translation control system and a magnetic attitude control system.

REVISIONS	LTR	DESCRIPTION	DATE	APPROVED

SECTION A-A

SECTION B-B

SCOUT P/L ENVELOPE 30° DIA

P/L ADAPTER INTERFACE

30.0

SEPARATION PLANE

PROPELLANT FIL VALVE	26
LO PRESS. TRANSDUCER	25
HI PRESS TRANSDUCER	24
SECOND STAGE REGULATOR	23
FIRST STAGE REGULATOR	22
THRUSTOR	21
PROPELLANT TANK	20
SOLAR CELLS	19
CAGING MECHANISM	18
PROOF MASS HOUSING	17
ANTENNA	16
SUN SENSOR	15
CORNER REFLECTORS	14
DESPIN SYSTEM	13
WOBBLE DAMPER	12
STAR SENSOR	11
HORIZON SENSOR	10
BATTERY	9
POWER CONDITIONING	8
MAGNET COIL	7
ATTITUDE CONTROL	6
TRANET	5
STADAN	4
COMMAND RECEIVER	3
TELEMETRY & PROCESSING	2
TRANSLATION CONTROL	1

DESCRIPTION	DWG. OR PART NO.	NO. REQ'D	ITEM NO.

UNLESS OTHERWISE SPECIFIED
1. DIMENSIONS IN INCHES AND DECIMALS
2. TOLERANCES .XXX±.01 .XXX±.005 ANGLES ± .25°
3. DRILLED HOLES +.002 −.001
4. MACHINED FINISH √MAX
5. MACHINED FILLETS .000 R. MAX
6. DIAMETERS CONCENTRIC WITHIN .05 TIR
7. DEBURR, REMOVE SHARP EDGES .005 MAX. R. OR CHAMFER
8. RESISTANCE IN OHMS, CAPACITANCE IN MICROFARADS

RELEASE DATE 6-19-70
CHECKED

MATERIAL

SURFACE TREATMENT

GUIDANCE & CONTROL LABORATORY
STANFORD UNIVERSITY

TITLE PRELIMINARY DRAG-FREE SATELLITE

SIZE D DWG. NO. GP-1

SCALE 1/4 SHEET 1 OF 1

76-A

76-B

FIGURE IV-15: PRELIMINARY DRAG-FREE SATELLITE LAYOUT

A pulsed plasma translation control design was also studied and yields significantly longer lifetimes and is described later. However, at the design altitude (1050 km) the cold gas system easily provides lifetimes on the order of a year or longer. The spherical propellant tanks are sized for 200 lb-sec of Freon 14 (I_{sp} = 40 sec) at 1500 psi and 100°F, all easily obtainable with standard techniques.

Figure IV-16 shows the lifetime and average control force levels vs orbit altitude for both the cold gas (200 lb-sec of propellant) system and the pulsed plasma (2000 lb-sec of propellant) system. The cross sectional area assumed in these calculations is based on the enlarged (42") SCOUT shroud which will be available in 1974.

The equipment list with estimated weights and power requirement is contained in Table IV-1. The estimated total weight of 146 lbs is comfortably within the 160 lb. capability for a polar SCOUT launch into a circular 1050 km orbit (Fig. IV-17). The average and maximum power requirements can also be met by locating solar cells on all satellite surfaces. The assumptions used in this analysis are outlined in Table IV-2.

Considerations in the design of translation controllers for spinning satellites are contained in Sections B and C, as well as Ref. 15. Attitude control of a spinning drag-free satellite has also been reported in a recent thesis [22]. A block diagram of the control system as needed for the preliminary design in Fig. IV-15 is shown in Fig. IV-18.

All components in the design layout have been placed in as symmetrical a manner as possible. Ideally, the satellite would consist of a homogenous spherical shell because the mass attraction force on the proof mass would then be zero for all proof mass positions within the cavity. This is impossible to achieve in the actual design, of course, but serves as a guide in locating components about the proof mass.

In the equipment list (Table IV-1), components have been divided into two categories: (1) those essential to satisfactory performance

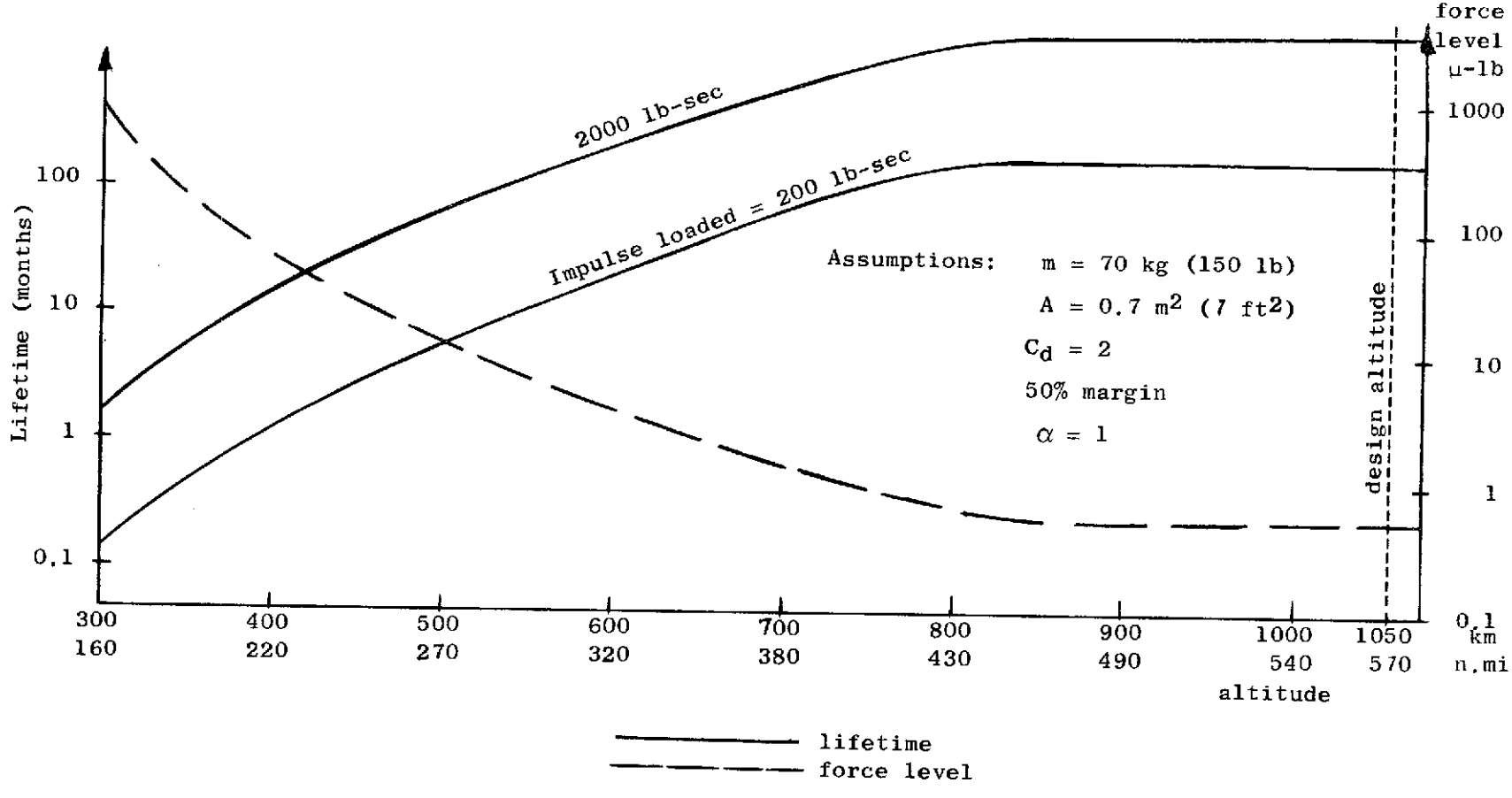

FIG. IV-16. LIFETIME AND FORCE LEVEL VS ALTITUDE

TABLE IV-1

EQUIPMENT LIST

Essential Components	Weight (lbs)	Power (watts) Maximum	Minimum
Structure	30		
Translation control electronics	5	3	3
Cold gas propulsion (200 lb-sec)	25		
Telemetry and other processing	10	5	5
Command receiver	2	1	1
STADAN (S-Band)	10	10	3
Attitude control electronics	5	2	2
Magnet coils	2	1	0.5
Power conditioning	5		
Batteries	7		
Solar panels	15		
Horizon sensor	3	1	1
Wobble damper	3		
Despin	3		
Components for Data Improvement			
Star sensor	6	1	0.5
Sun sensors	< 0.1	-	-
Corner reflectors	2	-	-
TRANET Doppler tracking	13	5	5
TOTAL	146 lbs 66 kg	29	21

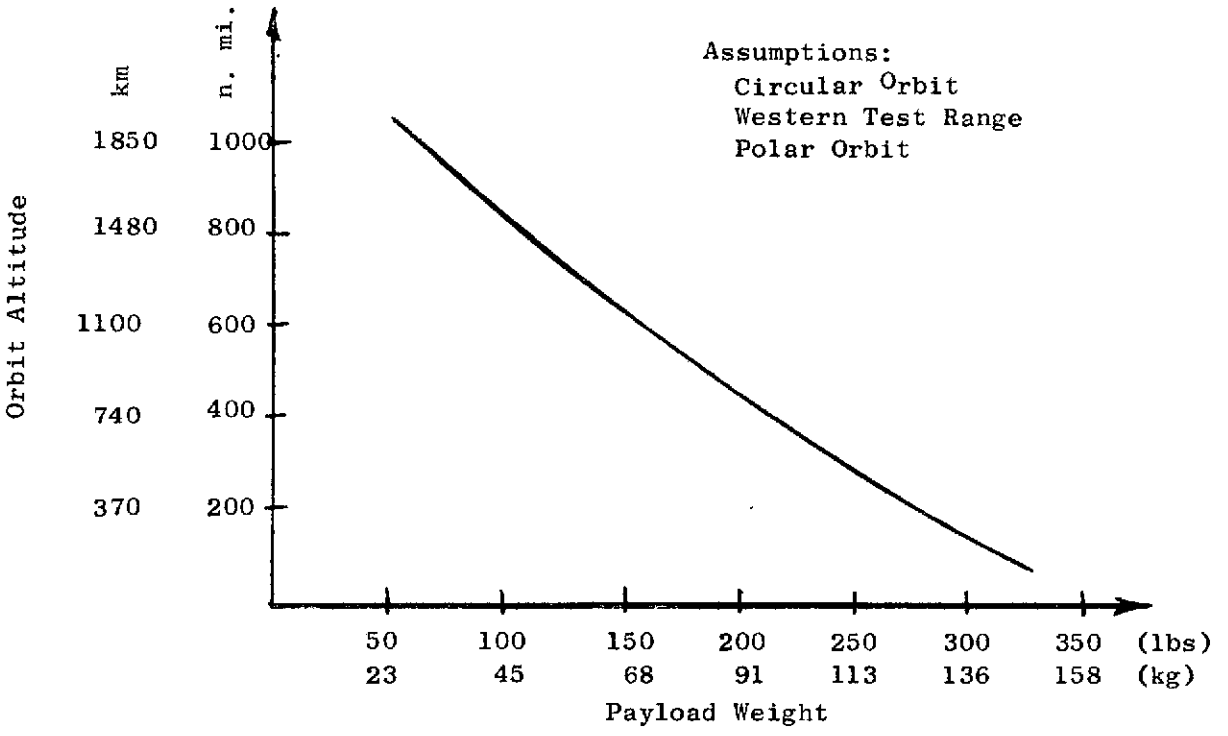

FIG. IV-18. SCOUT PERFORMANCE

Table IV-2

SOLAR CELL POWER

Assumptions
1. spin rate = 1 rpm
2. spin axis normal to orbit plane
3. solar cells on side $\leq 60^\circ \Rightarrow$ 45 mw/cell
4. solar cells on end $\leq 105^\circ \Rightarrow$ 35 mw/cell
5. minimum % of sun available: 0.65 (assumes orbital altitude $\gtrsim$ 200 n.mi.)
6. packing factor for sides = 0.85
7. packing factor for ends = 0.80
8. solar cell type: 2 × 2 cm, N/P, silicon 2Ω - cm, 12 mil thick active area = 3.9 cm^2
9. power loss in blocking diodes = 2 watts
10. area used by single cell in layout = 0.66 in^2
11. satellite is a 30-inch diameter cylinder, 30 inches long
Power Output - Sun Line Normal to Orbit
1. projected area = 705 in^2
2. usable projected area = (705)(0.8) = 564 in^2
3. number of cells = (564)/(0.66) = 850 cells
4. power in sunlight (and orbit average) = (850)(0.035) = 30 watts less 2 watts blocking diodes
5. Net Orbit Average Power: 28 watts
Power Output - Sun Line in Orbit Plane
1. projected area = 900 in^2
2. usable projected area = (900)(0.85) = 765 in^2
3. number of cells = (765)/(0.66) = 1150 cells
4. power in sunlight = (1150)(0.045) = 51.8 watts
5. orbit average = (51.8)(0.65) = 33 watts less 2 watts blocking diodes
6. Net Orbit Average Power: 31 watts

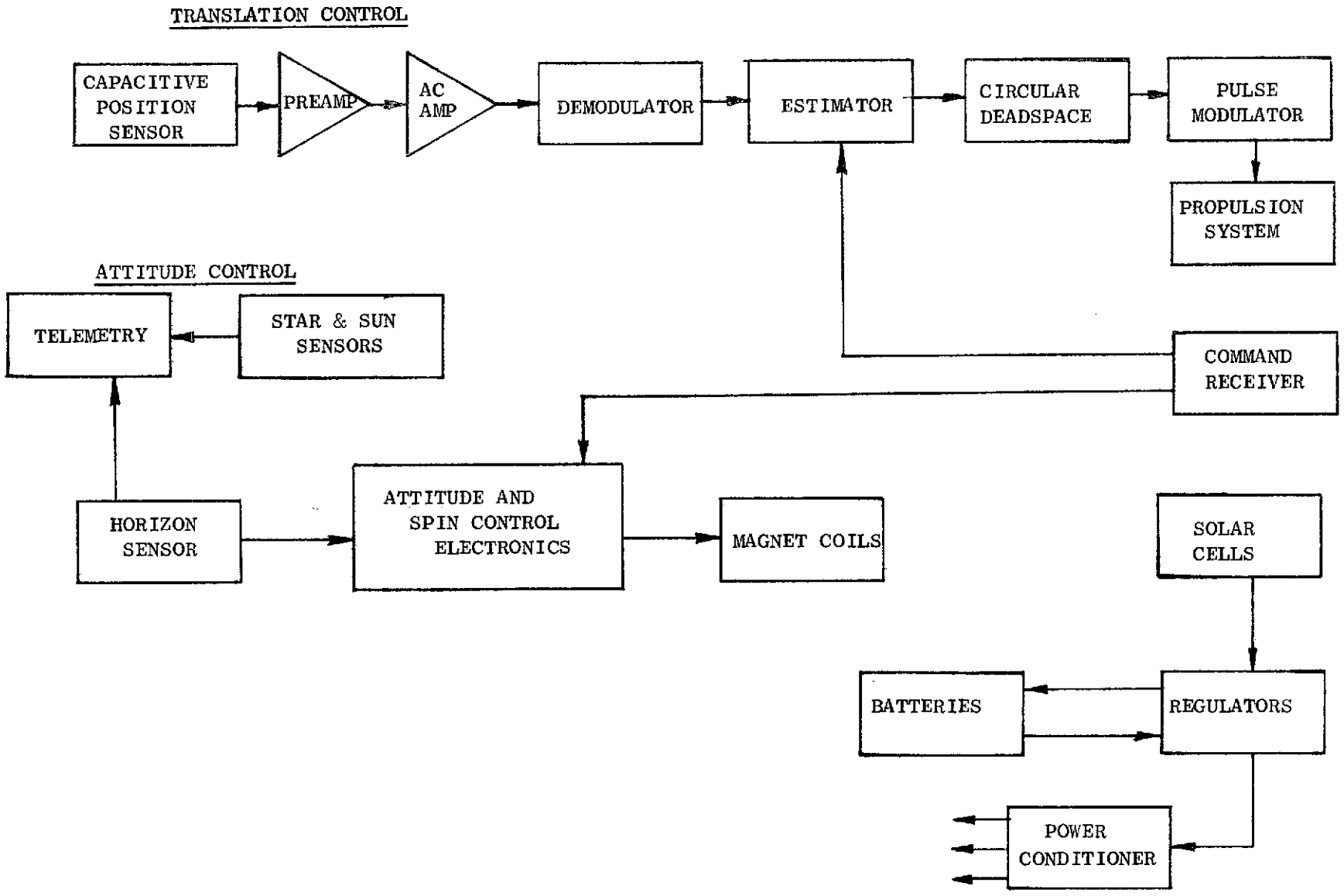

FIG. IV-18. CONTROL SYSTEM BLOCK DIAGRAM

of the satellite, and (2) those for data evaluation and improvement. In the latter category, the star and sun sensors would be beneficial to the data reduction by providing accurate attitude information. This information could then be used to correlate any observed systematic orbit errors with body fixed disturbing forces. The three sun sensors are inexpensive and very light weight and are therefore an attractive choice. The star slit sensor, while being substantially more accurate, is heavier, more expensive, and consumes more power; therefore, it becomes an optional component. The corner reflectors for laser tracking and the TRANET tracking system equipment both aid in establishing the orbit more precisely than that obtainable with the S-Band tracking system. Since the primary purpose of the geodesy mission is to extract useful information about the earth from the tracking data of the satellite, many accurate sources of tracking data will enhance the primary goal of the mission. Corner reflectors are light and consume no power, therefore, they should certainly be included. The TRANET Doppler tracking system would nicely complement the S-Band by allowing use of many more tracking stations. However, data availability would have to be established in sufficient time for proper interfacing of the equipment with the satellite.

6. Alternate Design

For low altitude missions designed for determination of the spatial gravity variations, a mission suggested by the Williamstown Study of August 1969 [Ref. 10], achieving satisfactory lifetimes is a critical area of study in drag-free satellite design. An alternate design was considered which is applicable to the low altitude mission. The propulsion system selected is the pulsed plasma system [Ref. 24] flown successfully on the LES-6 satellite. This design is shown in Fig. IV-19 and the equipment list given in Table IV-3. The lifetime of this design is plotted with the cold gas configuration in Fig. IV-16, and is longer due to the increase in impulse available. The power requirements in Table IV-3, however, are based on an average orbit altitude of 500 km. Mission altitudes below 500 km would require larger solar

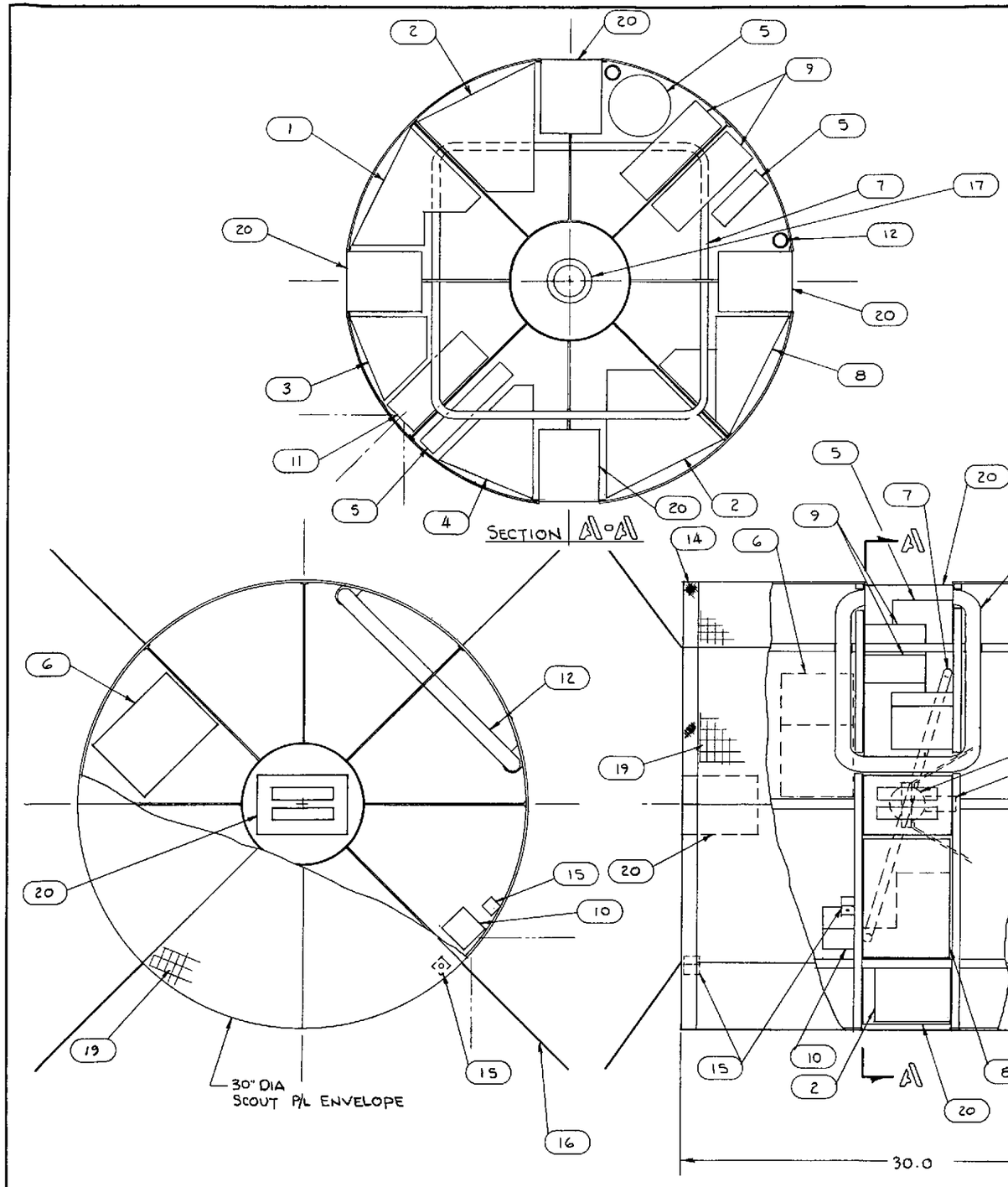

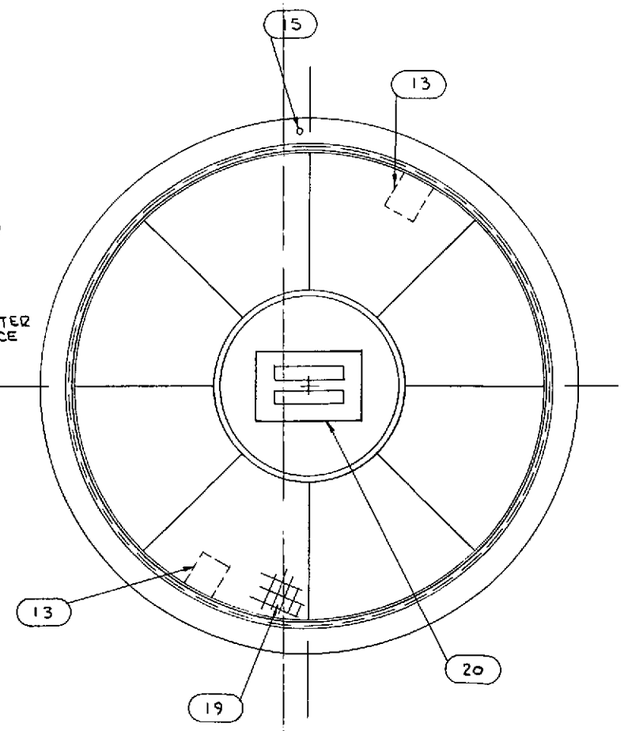

THRUSTOR	20
SOLAR CELLS	19
CAGING MECHANISM	18
PROOF MASS HOUSING	17
ANTENNA	16
SUN SENSOR	15
CORNER REFLECTORS	14
DESPIN SYSTEM	13
WOBBLE DAMPER	12
STAR SENSOR	11
HORIZON SENSOR	10
BATTERY	9
POWER CONDITIONING	8
MAGNET COIL	7
ATTITUDE CONTROL	6
TRANET	5
STADAN	4
COMMAND RECEIVER	3
TELEMETRY & PROCESSING	2
TRANSLATION CONTROL	1

DESCRIPTION | DWG. OR PART NO. | NO. REQ'D | ITEM NO.

REVISIONS | LTR | DESCRIPTION | DATE | APPROVED

UNLESS OTHERWISE SPECIFIED
1. DIMENSION IN INCHES AND DEGREES
2. TOLERANCES .XX±.01 .XXX±.005 ANGLES ±.25°
3. DRILLED HOLES +.005 -.001
4. MACHINED FINISH $\sqrt{}$ MAX
5. MACHINED FILLETS .005 R. MAX
6. RADIUSES CONCENTRIC WITHIN .05 TIR
7. REMOVE SHARP EDGES .005 MAX. R. OR CHAMFER
8. RESISTANCE IN OHMS, CAPACITANCE IN MICROFARADS

RELEASE DATE 6-21-70
DRWN.
DESIGN RH
CHECKED
MATERIAL
SURFACE TREATMENT

GUIDANCE & CONTROL LABORATORY
STANFORD UNIVERSITY

TITLE PRELIMINARY DRAG-FREE SATELLITE (PULSED PLASMA)

SIZE D DWG. NO. GP-2
SCALE 1/4 WEIGHT SHEET 1 OF 1

84-A

84-B

FIGURE IV-19: PULSED PLASMA DESIGN LAYOUT

TABLE IV-3

EQUIPMENT LIST

Essential Components	Weight (lbs)	Power (watts) Maximum	Minimum
Structure	30		
Translation control electronics	5	3	3
Pulsed plasma propulsion (200 lb-sec & 500 km orbit)	15	4	4
Telemetry and other processing	10	5	5
Command receiver	2	1	1
STADAN (S-Band)	10	10	3
Attitude control electronics	5	2	2
Magnet coils	2	1	0.5
Power conditioning	5		
Batteries	7		
Solar panels	15		
Horizon sensor	3	1	1
Wobble damper	3		
Despin	3		
Components for Data Improvement			
Star sensor	6	1	0.5
Sun sensor	<0.1	-	-
Corner reflectors	2	-	-
TRANET Doppler tracking	13	5	5
TOTAL	136 lbs 62 kg	33	25

arrays than those assumed in Table IV-2.

Most other features of this configuration are identical to the cold gas design features already discussed. An exception to this is the magnet coils for attitude torquing. The single skewed coil arrangement included in Fig. IV-19 was discussed by Sorensen [22] and is applicable to either drag-free satellite design. Although the single coil is lighter and usually consumes less power, the satellite may be less convenient to assemble with this arrangement.

F. SUMMARY AND CONCLUSIONS

In summary, it is recommended that to determine temporal variations in the gravity field:

(1) The orbit be

   a) of inclination 70° to 80° (to get at least one revolution of the node in a year);

   b) nearly circular;

   c) of 1050 km altitude (period 106.4 min., avoiding commensurability with anything less than a 27^{th} degree tesseral harmonic);

(2) The drag-free capability last at least one year;

(3) The tracking be from a distant satellite, if possible. But if from the ground, the stations should be well distributed, say, at least one per 90° × 90° × 90° quadrant of the globe.

For determining spatial variations, lower altitude operation is possible with drag-free satellites. The altitude selection is essentially a trade-off between tracking requirements, propulsion system capability vs lifetime, and the reduction in altitude which enhances the effects of the higher harmonics of the fixed gravitational field. Furthermore, a theory is being developed for nearly circular orbits which will facilitate data reduction for this type of mission.

The feasibility of all aspects of spinning drag-free satellite design have been established and most aspects demonstrated in the

laboratory. Some preliminary design has been accomplished for flight vehicles and the carryover of flight design from our work on the Navy's drag-free Navigation Satellite is significant. As a result of our design effort, we feel a first drag-free geodesy satellite can, and should, take advantage of spin as a means of lowering cost, and improving performance.

REFERENCES

1. "Proposal to Prepare A Preliminary Analysis and Design Definition of a Drag-Free Satellite for Geodynamics," submitted to the National Aeronautics and Space Administration by the Dept. of Aeronautics and Astronautics, Guidance and Control Laboratory, Stanford University, and the University of California at Los Angeles, March 1969; Addendum, May 1969.

2. B.O. Lange, "The Control and Use of Drag-Free Satellites," Ph.D. Dissertation, Dept. of Electrical Engineering, Stanford University Stanford, Calif., Jun 1964, SUDAER No. 194.

3. "Proposal for Phase I Studies of the Sustaining Orbiting Geophysical Observatory," vol. 1, Scientific/Technical, prepared by the University of California at Los Angeles, Institute of Geophysical and Planetary Physics Space Center for NASA, Dec 1962.

4. "First Semiannual Report on a Study to Prepare a Preliminary Analysis and Design Definition of a Drag-Free Satellite for Geodynamics," submitted to the NASA under Contract NSR-05-020-379, Stanford University, Guidance and Control Laboratory, Feb 1970.

5 Applied Physics Laboratory, Johns Hopkins University's contract to Stanford University in answer to Stanford's proposal: "To Develop and Build A Disturbance Compensation System for the Transit Satellite," Contract No. APL/JHU 271881, Jun 1969.

6. "Request for Continuation of Support of a Program to Perform a Gyro Test of General Relativity in a Satellite and Develop Associated Control Technology," submitted to the NASA by the Department of Physics, Stanford University, Aug 1969, Contract No. NGR 5 020 019.

7. "Interim Engineering Report of a Continuing Program of Advanced Research in Guidance, Control, and Instrumentation," Contract No. AF F33615-67-C-1245, by Stanford University, Guidance and Control Department, Stanford, Calif., 94305, Jan 1967 through December 1969.

8. "Final Technical Report on a Preliminary Design of a Drag-Free Satellite and Its Application to Geodesy," Stanford University, Guidance and Control Lab., and the University of California at Los Angeles, May 1969.

9. Munk and MacDonald, The Rotation of the Earth, 1960, p. 133

10. Seminar on "Solid Earth and Ocean Physics," at Williams College, Williamstown, Mass., sponsored by the NASA, Aug. 11-21, 1969.

11. Y. Kozai, "Effects of the Tidal Deformation of the Earth on the Motion of Close Earth Satellites," J. of the Astronomical Society of Japan, no. 4, vol. 17, Jul 1965.

12. A. Deprit, "The Main Problem of Satellite Theory for Small Eccentricities," Boeing Scientific Research Labs Document DI-82-0888, Aug 1969.

13. J.M.A. Danby, Fundamentals of Celestial Mechanics, Macmillan, 1962, p. 252.

14. C.M. Petty and J.V. Breakwell, "Satellite Orbits about a Planet with Rotational Symmetry," J. of the Franklin Institute, Oct. 1960, p. 259.

15. J.D. Powell, "Control of a Spinning Drag-Free Satellite with an Application of Estimation Theory," Ph.D. Dissertation, Dept. of Aeronautics and Astronautics, Stanford University, Stanford, Calif., May 1970, SUDAAR No. 402.

16. B.O. Lange, "The Drag-Free Satellite," AIAA J., vol. 2, no. 9, Sept. 1964, pp. 1590-1606.

17. P. Jhin, "Control of a Spinning Drag-Free Satellite to Reduce Trajectory Errors Due to Mass Attraction," Engineer's Thesis, Dept. of Aeronautics and Astronautics, Stanford University, Stanford, Calif., Aug 1970, SUDAAR No. 408.

18. R.N. Clark, "Analysis of Oscillations in Pulse-Modulated Satellite Attitude Control Systems," Ph.D. Dissertation, Dept. of Electrical Engineering, Stanford University, SUDAAR No. 361.

19. D.B. DeBra et al, "A Precision, Active, Table Leveling System," J. Spacecraft and Rockets, vol. 5, no. 9, Sept 1968, pp. 1040-1045.

20. A.W. Fleming, D.B. DeBra, and Crespo da Silva, M., "Attitude-Translation Coupling in Drag-Free Satellites," paper presented at the IIIrd IFAC Symposium on Automatic Control in Space, Toulouse, France, Mar 1970.

21. A.W. Fleming and D.B. DeBra, "The Stability of Gravity-Stabilized Drag-Free Satellites," AIAA Guidance, Control, and Flight Mechanics Conference, Santa Barbara, Calif., Aug 1970.

22. J. Sorensen, "Precision Magnetic Attitude Control of Spinning Spacecraft," Ph.D. Dissertation, Dept. of Aeronautics and Astronautics, Stanford University, Stanford, Calif., Aug 1969, SUDAAR No. 380.

23. W.J. Guman and E. Vogel, "Pulsed Plasma Microthruster Propulsion System Application Notes," Fairchild Hiller Report No. PCD-TR-69-1, Jan 1969.